GEOMETRY AND GROWTH OF GRABENS, LOWER RED LAKE CANYON AREA, CANYONLANDS NATIONAL PARK, UTAH

BY

ALBERT W. STROMQUIST

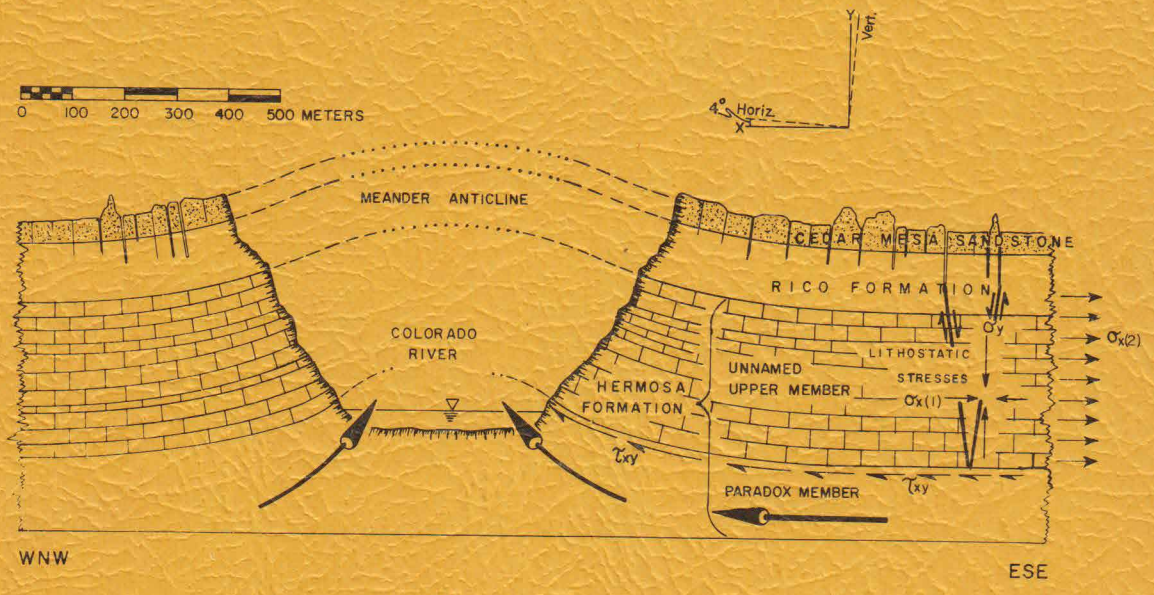

CONTRIBUTION NO. 28
DEPARTMENT OF GEOLOGY AND GEOGRAPHY
UNIVERSITY OF MASSACHUSETTS
AMHERST, MASSACHUSETTS

GEOMETRY AND GROWTH OF GRABENS, LOWER RED LAKE CANYON AREA, CANYONLANDS NATIONAL PARK, UTAH

By

Albert W. Stromquist

Contribution No. 28

Department of Geology and Geography

University of Massachusetts

Amherst, Massachusetts

September 1976

TABLE OF CONTENTS

ILLUSTRATIONS

ABSTRACT

During recent subsurface evaporite flow on the southeast side of the Colorado River in Canyonlands National Park, Utah, 460 m of brittle sedimentary rocks overlying the evaporite layer were faulted into a complex of narrow, closely spaced grabens extending for 25 km parallel to Cataract Canyon. Accelerated canyon cutting in late Quarternary reduced the overburden load confining the evaporites, thereby allowing the viscous material to flow down the gentle westerly regional dip and accumulate beneath Cataract Canyon. A horizontal tensile stress superposed on the regional lithostatic stresses by evaporite flow had sufficient magnitude to allow extension and normal faulting. Both the presence of evaporites and the gentle regional dip are essential to this mechanism for graben formation. Factors controlling the areal extent of faulting are a free face along Cataract Canyon, a pinchout of evaporites at the south end of the complex, a change in regional dip at the north end of the complex and an updip limit to evaporite flow to the east and southeast.

Grabens in the study area are several kilometers in length and range in width from 75 to over 400 m and in depth up to 140 m. Unslickensided fault scarps form vertical graben walls except where mass wasting has destroyed the original fault scarps.

The rocks possess a strong vertical fracture anisotropy that predates graben faulting. Two distinct trends are observable with orientations approximately parallel and transverse to the graben trend.

Wide-open master joints in each set break the bare rock surface into a rhombic grid.

Deep tributary canyons, incised transverse to the grabens, expose faults on the canyon walls. Study of several graben terminations on the walls of Lower Red Lake Canyon reveals that faults are vertical within 100 m of the surface, where displacement follows open master joints, but converge at depth with average dips of 85°. At close range the faults are observed to be a step-like succession of segments dipping 65° and 90°, in which the vertically dipping segments follow the preexisting fractures. A contrast in cohesive strength of individual beds is indicated, whereby beds with high cohesive strength fail by slip along vertical joints, and beds of low cohesive strength fail in shear along planes at angles of 25° to the maximum principal compressive stress. Grabens display good lateral symmetry with depth, requiring that the maximum principal stress had to be vertically oriented at all depths.

Fault geometry defines boundary conditions on a simple stress model for estimating average tensile strength of the brittle layer and the magnitude of a superposed shear stress due to evaporite flow. A range of overall tensile strength, normal to the strike of the grabens, is indicated to be between 11 and 17 bars. Lateral symmetry of the grabens requires that the shear stress superposed on the base of the brittle layer not exceed about 45 bars.

Many geometric similarities exist between Canyonlands grabens and grabens produced experimentally in a layer of dry sand and powdered limestone overlying a viscous layer of paraffin wax. Based on the

results of more than 20 model experiments, as well as field observations, the structural history of a typical graben is postulated by four stages of growth as follows: (1) Graben faults begin from a common location at or very near the brittle/ductile contact and propagate upward with 85° dips, thereby delimiting an incipient graben with a maximum width of 80 to 100 m at the surface. (2) The downthrown block subsides by equal and simultaneous displacements on both faults and propagates along strike with a constant initial width of 80 to 100 m. The upthrown block, downdip from the graben, detaches everywhere except at the ends of the graben and continues to creep downslope due to the force of gravity. (3) Propagation along strike declines, but extension continues and downfaulting is enhanced by internal failure of the graben block under its own weight. Secondary widening occurs as faults become unstable and joint-bounded slabs collapse away from the graben walls. (4) Extensive collapse along the sides of the graben obliterates the original fault scarps and contributes to the filling of the canyon above the graben. Internal failure and brecciation of the downthrown block continue. Accumulation of evaporites beneath the graben as a result of differential loading causes tilting and warping of adjacent upthrown blocks and leads to the growth of small grabens along the margins of the larger structure. During stage 2 another graben begins updip and the same process occurs. The result is a series of parallel, uniformly spaced grabens that become progressively younger updip from Cataract Canyon.

Trigonometric expressions for the amount of cross sectional area occupied by solids and voids at two successive times in graben development combine to yield a nonspecific quadratic equation relating the

following variables: (1) initial and final surface dimensions, (2) thickness of the faulted layer, and (3) the fractional volume increase of the original graben block (bulk dilation) due to megascopic voids formed by internal failure. When the equation is solved for thickness of the faulted layer, an expression is obtained for predicting depth to the flowing layer on the basis of surface geometry alone, assuming negligible bulk dilation. The expression is probably valid for a simple graben in which the original fault scarps were not destroyed by secondary widening.

INTRODUCTION

The Problem

Studies of a system of young grabens near the confluence of the Green and Colorado Rivers in Canyonlands National Park, Utah (Fig. 1) have shown that the method of estimating the depth of grabens as the depth of intersection of faults projected into the subsurface as planes dipping about 60°, is not reliable for near-surface grabens formed in brittle sediments overlying laterally spreading evaporites. These grabens have been described in a recent publication by McGill and Stromquist (1974).

The objectives of this investigation are to describe the features that characterize the grabens within this system and to propose a kinematic growth model that is compatible with observed geometry and the mechanical properties of the sedimentary rocks.

Sufficient evidence was gathered from detailed geologic mapping of a small area within the graben system and from work with geologic scale models to devise a model for graben formation, including a method for estimating the thickness of the faulted layer. Much time was consumed attempting to identify all the possible objections and in articulating the model so it would account for them. The result is a model that describes the origin and growth of grabens and which is consistent with the observable geometry in the study area. Nevertheless, there are still obvious anomalies and some very valid objections that remain unresolved.

Figure 1: Topographic map of The Grabens area reproduced from a 1:62500 U.S. Geological Survey (1969) map of Canyonlands National Park.

- -

Previous Investigations

The history of geologic investigations along Cataract Canyon and in The Needles fault area began with reports of the Powell Expeditions. Members of the expeditions of 1869 and 1871 described the Meander anticline along Cataract Canyon and were the first to photograph and study the graben system (Powell, 1875). No further work was published until Harrison (1927) studied the Cataract Canyon area as part of a regional investigation of salt domes in Colorado and Utah. Harrison proposed that the Meander anticline is a recent structure caused by flowage of subsurface evaporites into the axial region of the Canyon as a result of local loss of confining pressure with canyon cutting. Prommel and Crum (1927) published a similar study shortly after Harrison and took issue with his interpretation of the origin of the Meander anticline, attributing it instead to late Paleozoic folding and associated salt intrusion. Mutschler and Hite (1969) gathered new geophysical evidence which suggested that the location of Cataract Canyon is in part controlled by a Paleozoic lineament. Baker (1933, 1946) expanded Harrison's theory and proposed that the grabens formed in response to tensile stresses created by movement of evaporites down the west-dipping regional slope toward Cataract Canyon. This theory will be examined in a later section in light of new data. The grabens have been cited in reports of regional investigations by several other workers (Gregory,

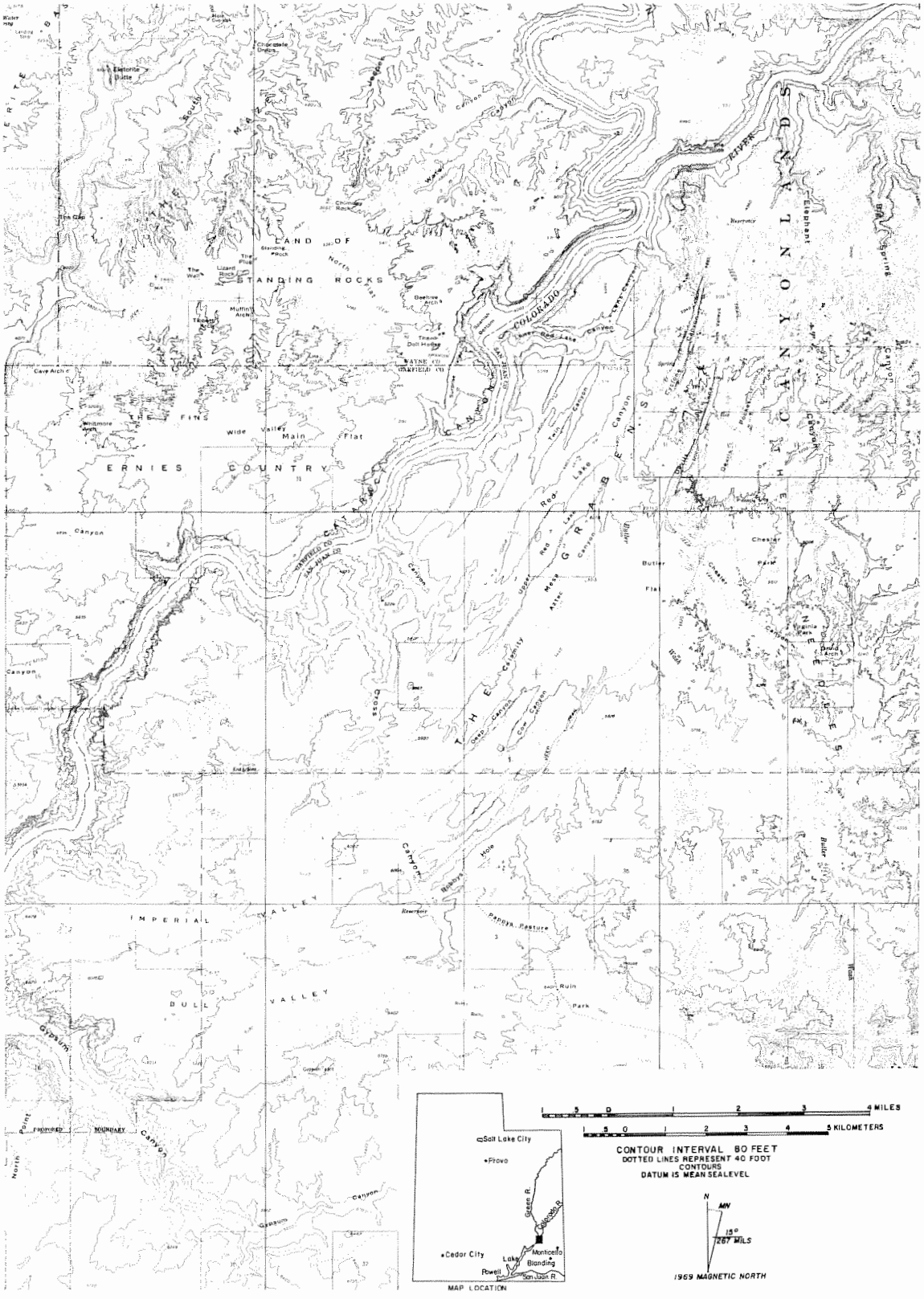
LAND OF
STANDING ROCKS
ERNIES COUNTRY
THE FINS
Wide Valley
Main Flat
COLORADO
GRAND CANYON
CANYONLANDS
IMPERIAL VALLEY
BULL VALLEY
Salt Lake City
Provo
Cedar City
Lake Powell
Monticello
Blanding
San Juan R.
Green R.
Colorado R.
MAP LOCATION
CONTOUR INTERVAL 80 FEET
DOTTED LINES REPRESENT 40 FOOT CONTOURS
DATUM IS MEAN SEALEVEL
1969 MAGNETIC NORTH

1938; Hunt, 1956; Kelley and Clinton, 1960). Lewis and Campbell (1965) summarized the work of earlier investigators and presented a generalized fault analysis. In addition, they inferred a geometric model which they used to estimate the required volume of displaced evaporites to account for the volume of the grabens. Baars (1971) contended that large volumes of evaporites were removed in solution by groundwater flowing down the nose of the Monument upwarp, thereby leaving voids into which the overlying rocks collapsed. McGill and Stromquist (1974) discussed the structural geology of the graben system with emphasis on the northeastern portion and examined Baker's hypothesis with respect to several possible subsurface geometries in light of field observations and work with geologic scale models. A description of the geology, geography, and anthropology of Canyonlands National Park (Lohman, 1974) has been recently published by the U.S. Geological Survey.

Geological and Physiographical Setting

The Canyonlands area occupies a position on the broad west flank of the Monument upwarp near its north-plunging nose. This is demonstrated by the gentle 3°-4° northwest regional dip observed within the field area. The graben system extends from about 1 km south of the confluence of the Green and Colorado Rivers for 25 km along an arcuate trend concave to the northwest and varies in width from 6 km to 12 km. The complex dies out to the west of Cross Canyon between Gypsum and Cataract Canyons. The area chosen for study covers a rectangular strip 4.5 km in the E-W direction and 2 km in the N-S direction, approximately centered around Lower Red Lake Canyon at the north end of the graben complex (Fig. 1).

Figure 2: View SSE of Lower Red Lake Canyon area. A prefaulting erosional surface is broken by two sets of vertical joints, elongate grabens downthrown between steeply dipping faults, and remnants of an older integrated drainage. The rocks have an average 3° to 4° west dip, except where dip reversal occurs along the southeast side of Cataract Canyon. UC = Unnamed Canyon graben; TC = Twin Canyon graben; LC = Lens Canyon graben; RLC = Red Lake Canyon graben; CC = Cyclone Canyon graben.

- -

The regional topography is dominated by an old, gently warped erosional surface with generally low relief except for isolated pinnacles of red sandstone up to 50 m high. Integrated dendritic drainages are developed to the east of the graben complex, but within the complex the present drainage is mostly internal, ending in swallow holes or small

ponded evaporation basins. Remnants of an integrated, prefaulting drainage are preserved on the intergraben divides.

The faulted area can be characterized as a bare rock surface of moderate relief. Much of this relief is of relatively late origin. Within this area the old erosional surface is broken by steep-walled grabens with smooth floors covered mostly by windblown sand and silt (Fig. 2). Graben depths vary from 0 to over 100 m below the erosional surface; however, the greatest relief occurs not along the grabens, but along Cataract Canyon and its tributaries where depths of 400 m are commonly exceeded. Changes in the topography are both numerous and abrupt, occurring most often as cliffs and steep talus slopes. These make foot travel away from established trails both slow and difficult.

Access by road to Canyonlands National Park is provided by following state highway 211 west from its junction with U.S. highway 163 about 14 miles north of Monticello, Utah. Once in the park, access to the grabens area can be gained only by foot, horseback, or four-wheel drive vehicle on well-marked trails. Motorized travel through the grabens is restricted to selected routes between valleys.

Methods

The structural analysis represents the cumulative results of detailed geologic field mapping and stereographic photo interpretation. Field work was done in April and May 1974. The data were plotted in the field on U.S. Geological Survey aerial photographs enlarged to an average scale of 1:8500. Geology was plotted on the fold-out map (Plate 1) with the aid of a Zeiss Stereotope and pantograph plotter.

Horizontal and vertical control was provided by the Carlisle 3 NE and Carlisle 3 NW 7-1/2 minute topographic quadrangles published by the U.S. Geological Survey (1955, preliminary editions). High- and low-angle oblique black and white and color photographs were used to aid in structural interpretation. In addition, several successful attempts were made to take strips of low-level overlapping vertical photographs (average scale 1:3000) in key areas, using a hand-held single lens reflex camera with a 58 mm lens. Geologic scale models were constructed in the laboratory during the summer and fall of 1973 and in the fall of 1974 and the winter of 1975. Both high-angle oblique and overlapping vertical photographs were taken of each model.

Acknowledgements

I wish to express my sincere appreciation to George E. McGill for providing the opportunity, the support, and the encouragement to perform and complete this research. George McGill's enthusiasm for teaching and his encouragement of a continuous exchange of hypotheses and criticism, enabled my research to evolve into an exciting academic experience. The manuscript was critically reviewed by George E. McGill, Alan W. Niedoroda, Stanley M. Bemben, Donald U. Wise, and Joseph H. Hartshorn. The research was supported by NASA Grants NGR-22-010-076 from the Office of Planetary Programs, and NGR-22-010-052 from the Apollo Lunar Exploration Office. Aerial photography was made possible with the assistance of Edward Zeller of the University of Kansas who provided both aircraft and skillful piloting. David Bond was my able field assistant. I am grateful to D. U. Wise for his professional and personal guidance, and to the many friends whose comments and suggestions helped to shape my research.

STRATIGRAPHY

The stratigraphic nomenclature used in this report is that of Lewis and Campbell (1965) and is in current use by the U.S. Geological Survey with only slight modifications in assigned ages (Lohman, 1974). The oldest rocks exposed within the map area are Middle Pennsylvanian evaporites that crop out at the mouth of Lower Red Lake Canyon. The youngest rocks are Lower Permian sandstones that form the present erosional surface. Unconsolidated eolian and alluvial deposits, often intimately interlayered on graben floors, together with extensive talus, are the youngest deposits in the area. Deeply eroded debris flows observed in Lower Red Lake Canyon are assumed to be of Wisconsin age (Hunt, 1956, p. 38).

Pennsylvanian System

Middle to Upper Pennsylvanian rocks in the field area are assigned to the Hermosa Formation. Two members have been identified in Cataract Canyon: (1) the Paradox Member (probably Desmoinesian) and (2) the unnamed upper member (Missourian to Virgilian) (Baars, 1971, p. 27).

Paradox Member of the Hermosa Formation. This unit is composed of evaporites, mostly gypsum and anhydrite, interlayered with dolomite and black shale. It is exposed at the mouth of Lower Red Lake Canyon, chiefly as a domical anhydrite intrusion with dolomite and shale occurring both as thin competent beds and as breccia in an intensely sheared anhydrite matrix. The unit weathers as steep talus-covered slopes and as cliffs where it is supported by more resistant beds. The weathering color is predominantly yellow. I believe that the original depositional

contact is locally preserved and that intense shearing is confined to strata at depths greater than about 10 m below the contact with the overlying upper member.

Unnamed upper member of the Hermosa Formation. The upper member is characterized by thick gray to green gray and buff cliff-forming beds separated by gray to light green gray talus slopes. The uniform weathering color is most obvious when the unit is observed from a distance. The upper member is composed of limestones interlayered with lesser amounts of sandstone and shale and attains a thickness of over 300 m in Lower Red Lake Canyon where it is entirely exposed. The limestones vary from thin bedded to thick bedded and massive, the latter being more common, and from crumbly slope formers to very resistant cliff formers. Light gray is the principal weathering color, but tan, reddish brown, purple, and dark gray are also common. Chert nodules and both large and small marine invertebrate fossils and fossil fragments, often chertified, are common but vary in occurrence from absent to very abundant. Fluvial type crossbedding is present but rare. Sandstone varies from fine to coarse grained, thin to thick bedded, and may weather deeply or form smooth continuous cliffs. Typical weathering colors are gray, mottled gray green, white, pink, and reddish brown to tan. Festoon crossbed sets are common. Shaly units are mostly thinly laminated and deeply weathered, usually forming reentrants when exposed. Calcite is the most common cementing material. The lower contact is taken to be the lowest fossiliferous limestone above yellow talus. The upper contact forms a prominent topographic bench at the top of a massive gray cliff, divided into three segments in the field area by

shallow reentrants. This bench characterizes the upper contact throughout the Lower Red Lake Canyon area. The upper contact also marks the transition from the predominantly red talus of the overlying Rico to the gray talus of the upper member of the Hermosa.

Permian System

The Permian system has been divided into the Rico Formation, a transitional facies from marine to continental sediments, and the conformably overlying Cedar Mesa Sandstone Member of the Cutler Formation.

Rico Formation. The Rico is represented in Lower Red Lake Canyon by 120 m of alternating marine carbonates and arkosic redbeds. The age of these rocks and their facies relationships with Permian carbonates and continental clastics and with Middle Pennsylvanian carbonates has not been firmly established. New terminology, based on detailed faunal studies, has been proposed to supplant the one currently in use by the U.S. Geological Survey (Baars, 1962). For a detailed discussion of the "Rico problem" see Baars (1962, p. 158-159). Both Baars (1962) and Lewis and Campbell (1965) have assigned a Lower Permian age to the Rico in central Cataract Canyon. Lohman (1974) places it on the Permian/Pennsylvanian boundary.

The upper half of the Rico Formation weathers as a vertical cliff, whereas the lower half weathers as a stepped slope with three prominent cliff-forming units 5 to 10 m thick. These three resistant units, together with several units in the upper cliff, provide excellent marker horizons everywhere in the map area and can be used to measure displacements very accurately (Fig. 3). The Rico is distinguished from the underlying upper member of the Hermosa by the dominant red appearance of

both the talus and the weathered bedrock. Individual units are generally thinner than in the Hermosa. Limestones are medium to dark gray or commonly purple, and weather light gray, pink, red, and reddish brown. Fossiliferous beds are sparse. Sandstones are fine to medium grained, thin to medium bedded, and generally show fluvial cross bedding. Calcite is the most common cement. Weathering varies from mottled light gray and pink to salmon, red, reddish brown, and tan. Smooth weathered surfaces are often deeply stained by manganese and limonite. Sandstones generally weather to slopes, except where held up by more resistant limestones. The top was taken to be the last limestone beneath massive, tan-weathering, crossbedded sandstone.

Cedar Mesa Sandstone Member of the Cutler Formation. The Cedar Mesa Sandstone is the most prominent stratigraphic unit in the area, forming the high cliffs along Cataract Canyon and its tributary drainages and the sheer walls of the grabens. Erosion along parallel joints has created tall spires that give The Needles area its name. Where two nearly orthogonal joint sets are strongly developed, a characteristic weathering form suggestive of toadstool caps has developed. The Cedar Mesa Sandstone is composed of fine- to medium-grained, subangular to rounded quartz grains cemented chiefly with calcite, and varies from light gray to tan, light brown, and reddish pink. Beds of thin, slabby, gray limestone of minor areal extent are interlayered with thick lenses of sandstone. Concretions are locally abundant. Both large-scale eolian and trough-type crossbedding are present, the latter being the most extensive. Lewis and Campbell (1965, p. B11) suggest that large-scale crossbedding indicates subaerial deposition, but Baars (1962,

p. 178) prefers a subaqueous shallow marine origin owing to the common occurrence of trough-type crossbedding, horizontal bedding planes, and occasional limestone and shale beds. The Cedar Mesa Sandstone forms the bare, sparsely vegetated erosional surface in the field area. It is pocked by numerous weathering pits filled with fine windblown sediments. These pits often fill with water during rainfalls. Lewis and Campbell (1965) estimate an original thickness of approximately 350 to 400 m, but except for pinnacles only about 40 m are present in the field area.

FIGURE 3. IDEALIZED COLUMNAR SECTION OF PALEOZOIC ROCKS EXPOSED IN LOWER RED LAKE CANYON.

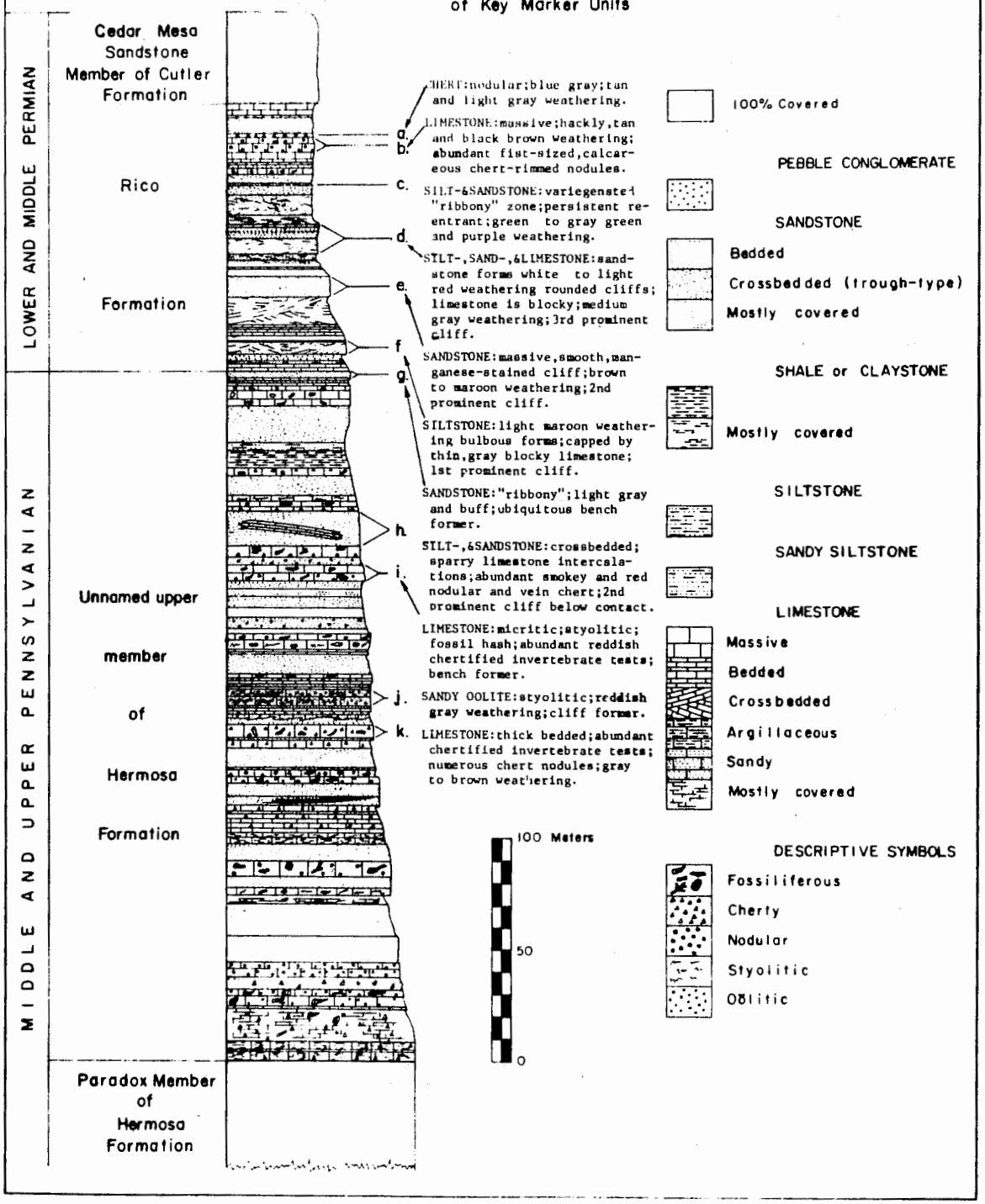

STRUCTURAL GEOLOGY

Description of Canyonlands Grabens

The interpretation of the origin and growth of grabens that has evolved out of this investigation is based largely on the detailed analysis of structure in the vicinity of Lower Red Lake Canyon. This implies that two important conditions are met: (1) that structures within the Lower Red Lake Canyon area are a representative sample of the graben system as a whole, and (2) that the model for origin and growth of grabens is valid for other areas within the graben complex where similar geometry is found. Thus, before any analysis of the structure within the study area can be attempted, it is important to discuss the entire complex of grabens with respect to such topics as: (1) the overall geometry of the complex, (2) variation in intensity of deformation as a function of distance from Cataract Canyon, and (3) the nature of the boundaries that have constrained the deformation. This will establish a framework within which the structural analysis of the Lower Red Lake Canyon area can acquire perspective.

Within The Grabens area (Fig. 4) the bedrock surface is broken by two distinct joint sets. One of these sets is closely parallel to the

- -

Figure 4: Location of joint stations and index to localities in the Lower Red Lake Canyon area. Each circular diagram represents an equal area stereonet and contains poles to 100 common joints plotted on the lower hemisphere. The structural geology of the numbered areas is described in the text. The scale of the photograph is approximately 1:49000.

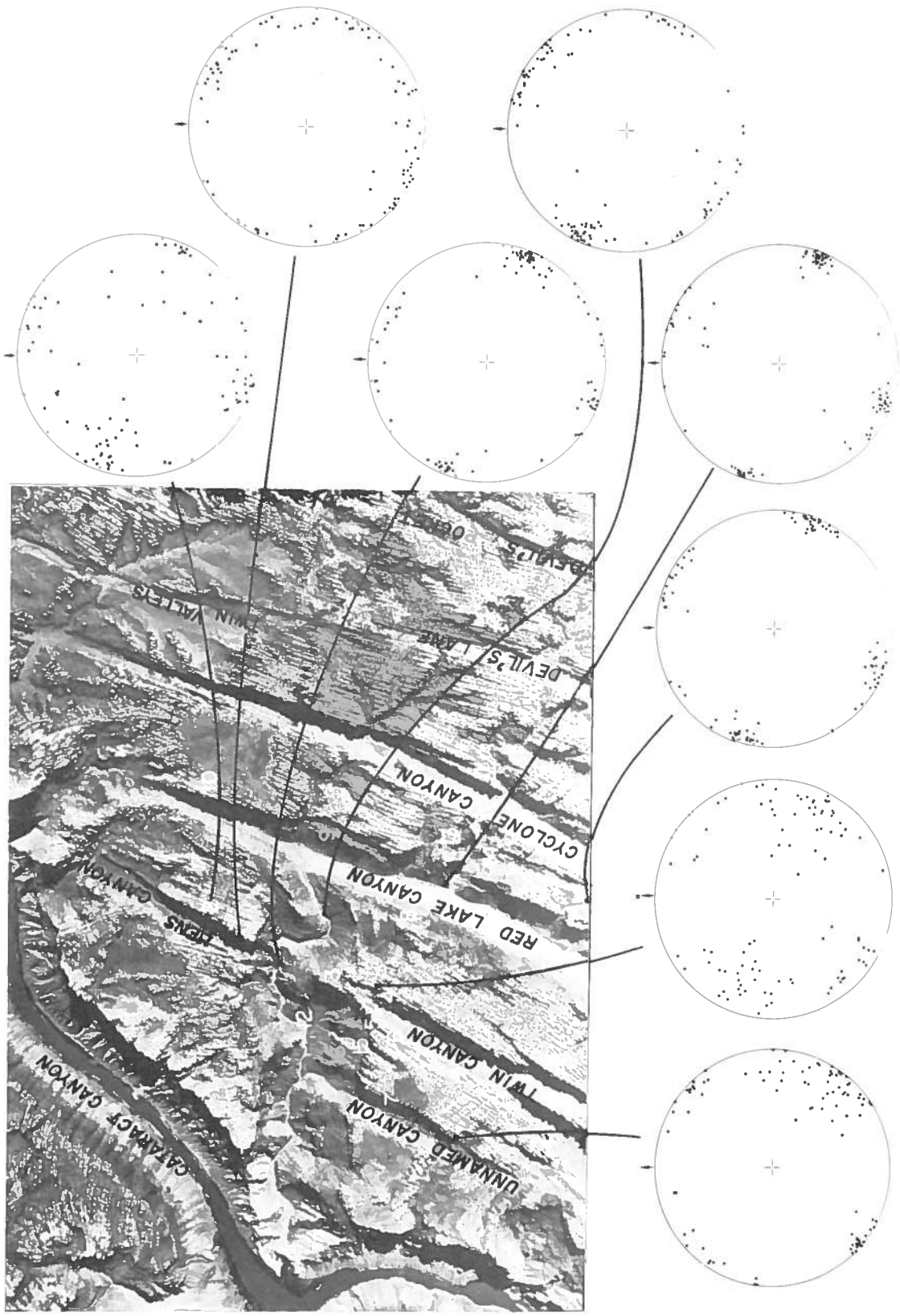
DEVIL'S LANE
CYCLONE CANYON
RED LAKE CANYON
TWIN CANYON
UNNAMED CANYON
CATAMACT CANYON

arcuate graben trend on the east side of Cataract Canyon, but turns to the northwest and west near the mouth of the Green River and dies out west of Cataract Canyon. East of The Grabens this joint set recurves to the northeast and strikes N40-50E. In the northern third of the graben system the rocks have been broken into obtuse rhombic blocks (Kelley and Clinton, 1960) by a second set of joints that strikes west-northwest. The joints are commonly opened as much as 2 m to depths up to 100 m. Several joint sets converge southeast of Chesler Park (Fig. 1) in a tightly knotted zone characterized by sharp curvature and complex intertwining of joint sets. A more detailed discussion of joints will follow in a subsequent section.

The grabens are contained in a belt with an average width of 10 km that lies to the southeast of Cataract Canyon. Between Lower Red Lake Canyon and Cross Canyon the strongest deformation is confined to within 5 km of Cataract Canyon. The grabens in this inner zone can be characterized as structurally complex. They are generally 100 m or more in depth, over 300 m wide, and have undergone extensive secondary widening by wall collapse and inward rotation of joint-bounded blocks. Thick talus accumulations are built out from the foot of the fault scarps. In addition, all of the anomalous uplift, tilting, and rotation of intergraben divides occur within this zone. The structure of the outer zone beyond 5 km and in the areas northeast of Lower Red Lake Canyon and southwest of Cross Canyon can be described as simple by comparison. The depths of the grabens rarely exceed 100 m and fall mostly in the range of 25 to 75 m. Widths are generally from 100 to 300 m. The fault scarps are only slightly modified by processes of

secondary widening and commonly have little or no talus along the base. Faulting dies out 5 to 6 km east of Cataract Canyon in the north end of the graben system and within 12 km southeast of Cataract Canyon in the vicinity of Cross Canyon.

The continuity of the 3° to 4° NW regional dip across Cataract Canyon is visible in structure contours drawn on the top of the Paradox Member of the Hermosa Formation (Elston and Shoemaker, 1961). The obvious lack of major deformation along the west side of Cataract Canyon, except for the Surprise Valley graben south of Spanish Bottom, is evidence for the importance of the regional dip to the structural development. South of the confluence of the Green and Colorado Rivers structural contours define a regional strike parallel to Cataract Canyon. However, anticlinal closure is indicated east of the confluence, which reflects the broad north plunging nose of the Monument upwarp. Where the graben system dies out along strike to the northeast, the regional dip turns from northwest to north and northeast parallel to the Colorado River. With the loss of gradient toward Cataract Canyon in this area, only the evaporites adjacent to the Canyon have intruded beneath the Canyon floor, otherwise the overlying sediments are not affected by Recent faulting.

Elston and Shoemaker (1961) also suggest that the Paradox Member pinches out along a northwest trending zone about 1 km southwest of Gypsum Canyon. The fact that the graben system dies out slowly west of Cross Canyon suggests that the transition may be governed by gradual stratigraphic pinchout of the evaporites rather than abrupt structural

pinchout (i.e., fault or fold). Moreover, no subsurface evidence is reported that would support structural pinchout.

Several internal boundaries are observed in the graben system that might have acted to constrain deformation. The most prominent of these is a strong northwest-trending fracture zone 12 km long (Fig. 5) that ends abruptly at Spanish Bottom. Along most of its length the fracture zone is a shallow syncline. A marked north to south transition in structural style is clearly observed across the zone. The pervasive rhombic fracture pattern that characterizes the northern third of the graben complex is present south of the fracture zone only as a weakly developed continuation of the east- to northeast-striking joint set. The effect is that the faults south of the fracture zone are not nearly as sharp as the faults to the north. In addition, there is no smooth continuity of a single graben across the fracture zone. For the purpose of this report, the fracture zone subsequently will be referred to as the Chesler Canyon lineament for the presence of the Chesler Canyon drainage incised along much of its length.

Other internal boundaries are in the form of fluvial canyons tributary to the Colorado River. The deeply incised sections of these canyons within 2 to 3 km of Cataract Canyon are of particular importance. Y Canyon, Cross Canyon, and Lower Red Lake Canyon are the most significant of these drainages because of their crosscutting relationship to large grabens in the complexly deformed inner zone. As part of the detailed description of Lower Red Lake Canyon, several lines of evidence will be presented to show that Lower Red Lake Canyon was incised nearly to its present depth before the area was faulted. Data for the Cross

Canyon and Y Canyon areas, however, are not sufficient to determine the relative age of either of these canyons with respect to the age of the faulting.

Introduction to Field Study in the Lower Red Lake Canyon Area

In order to characterize the geometry of the Canyonlands grabens, careful attention must be given to: (1) the attitude of the faults, (2) the effect of lithology on the dip of the faults, (3) the extent to which weathering and gravity driven processes have modified the fault scarps, (4) fault response at transverse discontinuities, (5) the orientation of the joints both at the surface and at depth, (6) the interaction of joints and faults, and (7) the relationship between the width and depth of graben. The Lower Red Lake Canyon area was chosen after a qualitative appraisal of aerial photographs to determine an area likely to yield maximum information bearing on these geometric topics.

The fact that structure at the ends of grabens is clearly exposed on the walls of Lower Red Lake Canyon establishes the canyon as a natural geologic structure section. It provides a means for direct observation of the geometry of faulting at depth. However, the structure of the graben walls could only be described as a representative cross section of grabens if the canyon was incised across the structural grain after the grabens had developed to their present size. It is likely that Lower Red Lake Canyon was deeply incised before faulting. Thus, if the canyon were a sort of internal boundary during the deformation, it is possible that the three-dimensional geometry observed in the canyon is different from that which would be observed on a cross section at some distance along strike away from the canyon. To

avoid bias which may have resulted from confining the study to the immediate canyon area, mapping was extended to include an area to the north, south, and east of Lower Red Lake Canyon in which structures formed in a stress system where the conditions of plane strain (Timoshenko and Goodier, 1951, p. 11-13) were closely approximated. Except for the extreme easternmost part, the field area lies within the complexly deformed inner zone.

Two major structural domains are recognized in the field area on the basis of characteristic style of deformation: (1) structure along the bottom of fluvial canyons, characterized by sinuous anticlines that follow the trends of the valleys; and (2) structures of the upland surface, characterized by major grabens and intergraben divides. The description of structure in the Lower Red Lake Canyon area will begin with an analysis of jointing and a discussion of possible origins for the joints and the relative age of joints and faults. Structure in the major domains will then be described in the order shown above.

Description and Analysis of Joints

Rocks of the upper member of the Hermosa, the Rico, and the Cedar Mesa are fractured by two pervasive joint sets. Master joints in the Cedar Mesa Sandstone have opened and have been subsequently widened and sculptured by weathering processes. Consequently, these joints appear as strong photolinears (Fig. 4). A systematic photoanalysis of the azimuth of master joints in the north end of the graben complex shows two distinct maxima with orientations of N15-30E and N55-70W (D. Leavell, pers. commun., 1975). The dips of these joints are vertical. Average spacing between master joints is 30 to 35 m with a range from 10 to

75 m. Poles to 100 common joints from each of eight sample localities plotted on equal-area nets (Fig. 4) show distinct maxima with the same orientations as master joints. The average dip of the common joints is greater than 80°. These joint stations were made only where the bedding dipped less than 3° and were chosen to obtain a representative sample of joint orientations at all levels in the stratigraphy. The nearly orthogonal relationship is demonstrated by measuring the acute angle between intersecting master joints on air photographs. A characteristic value for this angle is 80° or more. The simple assumption is made that the two joint sets originated as extension fractures.

Two possible explanations can be offered for the origin of systematic orthogonal joint sets. Price (1974) has developed an idealized stress model that predicts the conditions under which orthogonal tensile fractures may form parallel to the major and minor axes of a sedimentary basin that is either subsiding and compacting under the weight of continuously deposited sediments, or subjected to uplift and actively eroding. In this model, "knotted" joint sets could be attributed to local stress reorientations due to the effect of basement topography or to synsedimentary faulting. Broad curvature, on the other hand, might reflect differential rates of uplift or subsidence.

As an alternative model, Kelley and Clinton (1960, p. 63) have suggested that orthogonal joints in the Paradox Basin, like those in Canyonlands, may be the result of early movement of evaporites following Cutler deposition. This model is supported by studies in the salt anticline region of the Paradox Basin, which show that diapirism may

have been active as early as late Pennsylvanian (Harrison, 1927; Baker, 1933; Elston and Shoemaker, 1963). The Kelley and Clinton model provides simpler explanations for local changes in principal stress trajectories than does the Price model. It has been suggested by Kelley and Clinton (1960, p. 64) that the oval-like joint pattern around Cataract Canyon near Spanish Bottom may be due to some early piercement flow (upper Pennsylvanian-lower Permian) long before the canyon was eroded.

A first glance at an aerial photograph of the north end of The Grabens (Fig. 4) would suggest that the fault trends are controlled by the N15-30E joint set. A systematic analysis of the strike of all joints in the north end of the graben system has shown that the average strike of the faults corresponds to this joint direction (D. Leavell, pers. comm., 1975). Careful examination reveals that the strikes of these two tectonic elements are not always equivalent. Commonly, faults conform to open master joints in the surface rocks as a series of en-echelon segments along the N15-30E joint direction connected by cross faults utilizing the northwest-trending joints. When viewed in plan, the effect is a sawtooth pattern along the fault scarps.

It can be demonstrated that the joints predate the faulting by applying conditions of the theory of elasticity. Since tensile fractures form perpendicular to the least compressive stress, the intermediate and greatest principal stresses must be contained in the plane of the fracture. One of these principal stresses must be perpendicular to the fault scarps to satisfy the condition of no shearing stress on a free surface (Anderson, 1951, p. 12). This requires that one set of extension

joints intersects the fault scarps at right angles if the jointing postdates faulting. Because fractures in the N15-30E joint set intersect the fault scarps at a small acute angle, theoretical considerations require that the joints are older than the faults.

Structure Along the Bottom of Fluvial Canyons

The existence of the Meander anticline has been well established since it was first reported by the Powell expedition of 1865. Since then most workers in the area have accepted Harrison's (1927) hypothesis that it is a relatively recent feature or at least represents the effect of rejuvenated evaporite flow after an initial episode of diapirism in the late Paleozoic or early Mesozoic (Kelley and Clinton, 1960, p. 64). The presence of an evaporite ridge beneath Cataract Canyon (McGill and Stromquist, 1974, Fig. 7) is postulated on the basis of exposures of sheared evaporites for 16 km along Cataract Canyon (Lewis and Campbell, 1965, p. B31).

Hollingsworth and others (1944) reported the occurrence of valley bulges bearing strong similarity to the Meander anticline within the Northampton Ironstone Field, England. Competent limestones and marls in river valleys have been folded into anticlines that follow the trend of the rivers. Several cross sections show clay ridges and clay diapirs beneath the river valleys. The authors conclude that: (1) differential loading of the incompetent Lias clay developed as rivers incised the overlying brittle strata, (2) the clay flowed down the regional dip beneath the cover rocks in response to the uneven loading and accumulated beneath the river valleys, and (3) clay accumulation

produced arching of the overlying sediments in the form of sinuous anticlines that conform to the course of the valleys that they follow.

Cataract Canyon is subparallel to the regional strike and is therefore perpendicular to the direction of salt flowage. It is rather easy to imagine how an evaporite ridge could form beneath a nonuniformly loaded zone with such an orientation. However, a meandering anticline oriented parallel to the regional dip also follows the drainage in Lower Red Lake Canyon along the section west of Twin Canyon (Fig. 6). Dips on the limbs of the anticline in the lowest beds are generally less than 10° in the east end and gradually increase westward. As in Cataract Canyon, the dips decrease both upward and outward away from the canyon floor. Individual beds could be traced across the valley floor and show no evidence of either reverse or normal faulting indicating that only simple arching has occurred. The high-angle reverse faulting and subsequent collapse reported by Hollingsworth and others (1944) from the Northampton Ironstone Field is absent along Lower Red Lake Canyon.

The Lower Red Lake Canyon anticline and the Meander anticline culminate in the mouth of Lower Red Lake Canyon as a dissected dome cored by black shale and evaporites (Fig. 7). Tight isoclinal folding and a strong flow foliation visible in the core rocks provide evidence for the intrusion of very mobile Paradox strata. Steeply dipping beds of the lowermost upper member of the Hermosa enclose the core on three sides. The dips of units just beneath the upland surface at the junction of the two canyons similarly show the combined effect of both anticlines.

The importance of the Lower Red Lake Canyon and Meander anticlines is to demonstrate that flow has, in fact, occurred within the Paradox

Figure 5: Chesler Canyon lineament, looking west-northwest. CC = Chesler Canyon; SB = Spanish Bottom; LRC = Lower Red Lake Canyon.

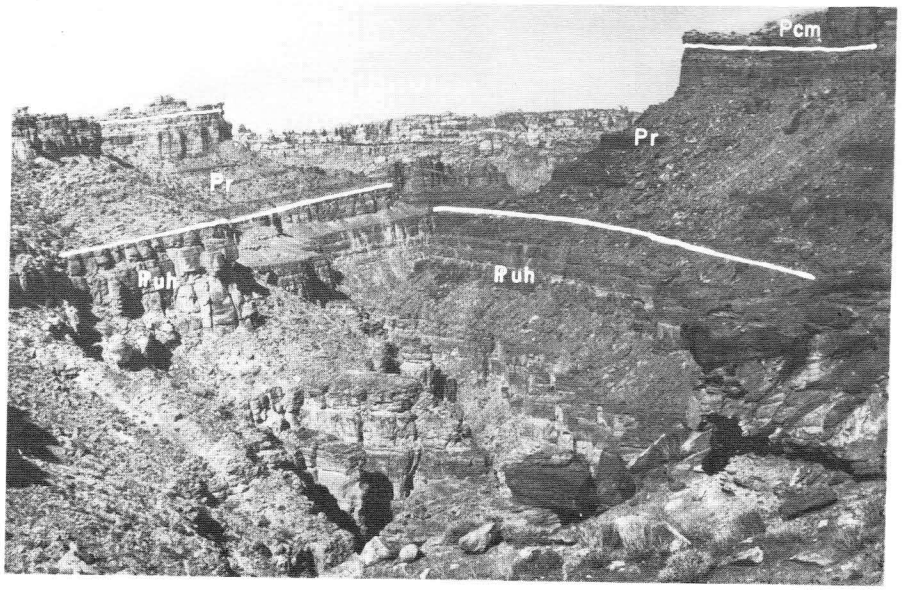

Figure 6: Lower Red Lake Canyon anticline, looking west toward Spanish Bottom. The anticlinal axis follows the meandering stream bed on the Canyon floor. Puh = upper member of the Hermosa Formation; Pr = Rico Formation; Pcm = Cedar Mesa Sandstone (Cutler Formation).

Member. Dome-like exposures of sheared gypsum as at the mouth of Lower Red Lake Canyon provide direct evidence for the mobility of Paradox strata. The close correspondence between the anticlines and the trend of the canyons, and the fact that anticlines do not normally meander, make it unlikely that the canyons were incised along the axes of preexisting anticlines. Therefore, Harrison's theory, that arching occurred as a result of downcutting in the canyons, is certainly more reasonable.

Discussion: Age of Lower Red Lake Canyon

Since subsurface flow is governed in part by differential loading on the evaporites, Cataract Canyon must have been deeply entrenched to allow the mechanism to operate. McGill and Stromquist (1974, p. 42) estimate that the thickness of the upper member of the Hermosa beneath Cataract Canyon was reduced to 50 m when flow began. It is a reasonable assumption that the declivity established in Lower Red Lake Canyon, allowing the two streams to intersect at a common level, was maintained during earlier times. From this assumption it is inferred that Lower Red Lake Canyon was entrenched to a similar depth when flow began. This is the most important argument favoring the prefaulting age of Lower Red Lake Canyon. In addition, well-cemented debris flows dissected by modern gullies were observed on the north wall of the canyon. The flows reach the present stream bed, where they are up to 5 m thick. Debris flows along the canyon of the Colorado River east of Hite, Utah, have been correlated with pluvials during the latest glaciation (Hunt, 1956, p. 38). The fact that graben faults are relatively unweathered and no

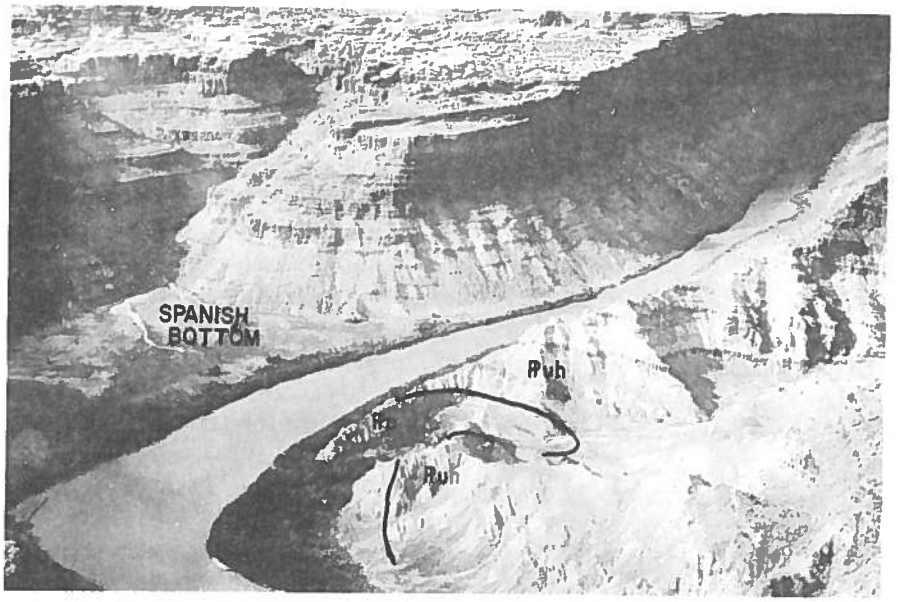

Figure 7: Evaporite plug in the mouth of Lower Red Lake Canyon. Stream erosion has exposed the core rocks that consist of isoclinally folded thin shale and dolomite beds and shale breccia in an intensely sheared evaporite matrix. Pp = Paradox Member of the Hermosa Formation; Puh = upper member of the Hermosa Formation.

other debris flows were observed along the fault scarps supports, in a circumstantial way, the prefaulting age of the canyon. Finally, it will be shown in a later section that none of the grabens exposed on the walls of Lower Red Lake Canyon continue uninterrupted across the canyon floor. Although several faults were projected southward across the floor of the canyon from the south end of the Lens Canyon graben, displacement on them is generally small on the south wall of Lower Red Lake Canyon. One way to account for this observation is by the presence of a transverse discontinuity that suppressed the propagation of fractures along trajectories at high angles to it.

Structure of the Major Grabens

The grabens in the vicinity of Lower Red Lake Canyon range in width from 75 to over 400 m. The depth of the graben floors beneath the surface of the intergraben divides ranges from 0 up to 140 m. The bedrock floor is generally covered by a blanket of alluvial and eolian deposits. Although exposures of bedrock on graben floors are rare, previous workers have assumed that the depth to the graben floor is a good approximation of the amount of vertical displacement (Baker, 1933, p. 74). It is difficult to estimate the magnitude of error in this assumption, as there is no effective way to systematically measure the thickness of young deposits.

At the surface, the unslickensided fault scarps, defined largely by vertical joint faces, show little effect of weathering, particularly where the grabens are less than 100 m in depth. However, in many cases the fault scarps are not simple, but have been modified by wall collapse and by inward rotation of joint-bounded blocks, so that the true spacing between the major bounding faults is masked by thick talus prisms. To be accurate, the term fault-line scarp should be used for these cases, but since the distinction is not always obvious in the field, the term fault scarp will be used hereafter in a general way. Specific ways in which fault scarps may be modified will be shown in detailed descriptions of individual grabens.

The reader will find it helpful to refer to Plate 1 and the numbered localities on Figure 4 to follow the descriptions of grabens and intergraben divides. The various marker beds used to describe fault

displacements are identified by lower case letters to the right of the stratigraphic column (Fig. 3).

Lens Canyon graben. The Lens Canyon graben extends northeast from Lower Red Lake Canyon along an average N30E strike for 2.2 km. The structure terminates northward on the south wall of a deep tributary canyon (Fig. 4, loc. 1). Displacements at the north end were observed to die out northward within the Rico Formation, such that the Rico/Hermosa contact on the canyon wall is unfaulted. The dip of the east fault at this location is vertical above marker e, but dips westward between units e and g at 53° before dying out. Displacements on the east and west faults at the north end of the structure range from nothing in the lower Rico to 10 m in the Cedar Mesa Sandstone. Displacements increase rapidly southward so that the exposed Rico and Cedar Mesa forming the graben floor in the north end, disappear southward beneath alluvial and eolian fill.

The joints in the vicinity of Lens Canyon diverge strongly from their regional trend. The N15-30E set turns sharply northwestward to cross Cataract Canyon near the confluence of the Green and Colorado Rivers. The effect of the divergent trends is a sharp sawtooth pattern on the fault scarps (Fig. 4, loc. 2). The east fault has a consistent N30E strike and forms a vertical scarp up to 100 m high. A talus prism extends across the full width of the graben floor. The west fault forms a very irregular scarp which varies from about 60 m high at the north end to only several meters at the south end.

Over most of its length, the graben has a smooth floor covered with alluvial and eolian sediments and is bounded by two well-defined fault

scarps. However, near the south end of the graben, the effect of joint divergence is to widen the graben on a series of right en-echelon extensions of the west fault. Where the structure intersects Lower Red Lake Canyon, a complex pattern of north- to northeast-striking faults developed. These faults are interconnected by cross faults formed along the N60-70W joints and outline several fault blocks in the Rico-Hermosa section on the north wall of Lower Red Lake Canyon. The structure at the south end of Lens Canyon is illustrated on a photomosiac (Fig. 8) assembled from a series of overlapping vertical photographs taken at low altitude with a hand held camera. Figure 8 illustrates some important observations that bear on the kinematic interpretation of graben development.

At location 1 (Fig. 8) Cedar Mesa Sandstone forms the floor of the graben and is exposed as a small keystone block in a gully following the east fault. In the field the east fault is clearly exposed below the Rico-Hermosa contact as a sheared and brecciated zone with a measured dip of 83° west. Displacement at this locality is at least 120 m. The southern limit of the relatively simple graben structure is shown as a north trending fault between locations 1 and 2 (Fig. 8), but the principal west boundary fault is taken to be a second north trending fault between locations 2 and 3. Although some of the fault curvature is not real, but due to extreme parallax, the downward convergence of graben faults is established for the Lens Canyon graben by direct observation in the field.

The Lens Canyon graben shows a pronounced asymmetry in the south end (Fig. 8, loc. 2). Displacement on the east fault of the graben is

Figure 8: Detail of faulting in the south end of Lens Canyon graben. Numbered localities on the photograph are keyed to the description of the fault geometry in this area. Puh = upper member of Hermosa Fm.; Pr = Rico Fm.; Pcm = Cedar Mesa Sandstone Member of the Cutler Fm.; Ra = Recent alluvium and colluvium.

U/D normal fault, showing displacement sense, located accurately

normal fault, approximately located

normal fault, location inferred

thrust fault, hachures on the upthrown block

contact, accurately located

γ_9 strike and dip of bedding

estimated between 60 and 70 m, whereas displacement on the west fault between locations 2 and 3 (Fig. 8) is about 25 m. The reason for this asymmetry will be discussed below. It was also observed that the rocks at both locations 2 and 3 are structurally continuous with beds on the south wall of Lower Red Lake Canyon. No evidence of major east-west cross faulting was found between the north and south walls of Lower Red Lake Canyon. Both the east and west faults of the Lens Canyon graben were traced across Lower Red Lake Canyon and found to converge and die out on the south wall of Lower Red Canyon near marker d (Fig. 8, loc. 6). This is the only location in Lower Red Lake Canyon where faults can be traced from the end of a graben to the opposite wall of the canyon. Finally, Figure 8 illustrates that while individual segments of the west fault die out along open master joints, the overall structure is continuous along right en-echelon faults (Fig. 8, loc. 5). This is an extreme example of the nonparallelism of joint and fault trends.

The south end of the Lens Canyon graben is an area of significant relative displacement of intergraben divides. Section B-B' across Lens Canyon shows structural relief of about 25 m from east to west. Two relative displacements are involved: (1) uplift and northeastward tilting at the south end of the Lens Canyon-Red Lake Canyon intergraben divide, and (2) broad eastward tilting of the upland surface between Lens and Cataract Canyons and downbending and faulting of the southeast corner of this block (Fig. 8, loc. 4). Continuity of the Cedar Mesa erosional surface is restored northward along Lens Canyon.

Numerous small faults were mapped near the floor of Lower Red Lake Canyon (Fig. 8, locs. 8, 9, 10). Displacement on most of the small faults is less than 10 m. A single large-scale fault with a measured displacement of 50 m down on the west was mapped on the south side of the stream bed in Lower Red Lake Canyon (Fig. 8, loc. 7). The presence of the faults establishes this area as the southeast corner of the Lens Canyon-Cataract Canyon divide. Although the extent of faulting is obscured by thick talus and alluvium along the canyon floor, the overall sense of the faulting and the magnitude of displacement, where determined, suggest an asymmetric graben. The geometry of the structure is analogous in some respects to the south end of the Lens Canyon graben, suggesting that this structure may be an en-echelon extension of Lens Canyon.

It is suggested that the complexity of the faulting in the south end of Lens Canyon is not characteristic of structures in the graben system, but is controlled by the presence and morphology of Lower Red Lake Canyon in the vicinity of Lens Canyon.

Twin Canyon graben. The Twin Canyon graben begins as a narrow, 40- to 50-m-wide, shallow structure on the rim of Lower Red Lake Canyon (Fig. 4, loc. 3). Both faults bounding the graben die out northward and are lost in talus on the south wall of Lower Red Lake Canyon. Displacements at this locality are about 22 m on the west fault and 12 m on the east fault. The graben extends southwest for 1.6 km along a N30E strike and then bifurcates into east and west branches off the map.

Where Twin Canyon is narrowest at its northern end, the alluvial-eolian cover characteristic of the graben floor is not present. The

downfaulted strata are seen not as a coherent block, but instead as a disordered array of joint-bounded blocks that vary both in magnitude of displacement and in strike and dip (Fig. 4, loc. 4). South of this area the graben widens westward on a series of right en-echelon hinge faults. These faults apparently die out northward in the Rico on the south wall of Lower Red Lake Canyon.

A small graben formed on the west side of Twin Canyon (Fig. 4, loc. 5) is contiguous with the major structure, but is separated from it by a narrow septum (Fig. 4, loc. 6), also structurally lower than the adjacent intergraben divides. A maximum displacement of 27 m down on the east was measured on the west fault at the rim of Lower Red Lake Canyon. At this location the graben attains a maximum width of 85 m. The west fault dies out northward as a faulted drag fold on the south wall of Lower Red Lake Canyon (Fig. 9). Here the east fault curves to the northwest and converges with the west fault above marker h. The graben extends 750 m southwest from the rim of Lower Red Lake Canyon and dies out as a north dipping ramp that merges with the surface of the Twin Canyon-Unnamed Canyon intergraben divide. At least two left en-echelon scissors faults tie the east fault of the small graben to the pricipal west fault of Twin Canyon.

Unnamed Canyon graben. The Unnamed Canyon graben extends southward 1.8 km from Lower Red Lake Canyon along a N20-25E strike. As in other grabens, the dips of the faults are vertical to a depth of at least 100 m, below which the scarps are buried by talus.

The graben is dissimilar in some respects to grabens described above. The maximum width is 235 m along the rim of Lower Red Lake

Figure 9: Faulted drag fold on the south wall of Lower Red Lake Canyon, looking southeast. The structure is the northward continuation of a small graben west of and contiguous with the Twin Canyon graben. The bench at the top of the massive cliff in the foreground is the Rico-Hermosa contact. Displacement on the fault dies out northward. Pr = Rico Fm.; Puh = unnamed upper of the Hermosa Fm.

Canyon. Measured displacement of Cedar Mesa Sandstone exposed in the floor of the graben is over 110 m. The displacement on both faults must die out rapidly northward, because the faults could not be traced across the stream bed in the floor of Lower Red Lake Canyon. The true width of the graben, that is, the spacing between the principal bounding faults,

is almost certainly less than the observed width. Thick talus prisms at the foot of both fault scarps, separated by a narrow alluvial-covered floor, suggest that this graben has undergone secondary widening by extensive collapse along the faults. Along the east fault in particular, a joint-block row 550 m long and about 30 m wide has been downfaulted and rotated inward so that it dips 31° toward the graben floor (Fig. 4, loc. 7). A detailed example of this type of secondary widening will be shown for a similar structure in Red Lake Canyon.

Grabens like Unnamed Canyon with narrow floors and little or no exposure of Cedar Mesa Sandstone have led some investigators to speculate that the supposed graben structures might really be no more than wide-open tension gashes (Kelley and Clinton, 1960, p. 64). However, at the south end of Unnamed Canyon, the graben floor emerges from beneath the alluvial-eolian cover as a north dipping ramp along which faulting dies out southward. The fact that downfaulted Cedar Mesa Sandstone is found at the north and south ends of Unnamed Canyon requires that it be present everywhere along the length of the graben, although buried by an undetermined depth of young deposits.

Red Lake Canyon graben. On the basis of its size alone, Red Lake Canyon is an anomalous structure within the graben complex. The width between canyon walls commonly exceeds 500 m and the depth of the floor beneath the surface of the divides reaches 140 m, thereby exposing nearly the entire thickness of the Rico and the uneroded Cedar Mesa Sandstone along the walls. Furthermore, the graben can be traced as a continuous structure for more than 9 km. Attributes which have clearly distinguished other structures as grabens, such as ramping joint block

rows at the ends and exposed bedrock on the floors, are either not found in Red Lake Canyon or are not definitive where observed. Thus, it was necessary to describe the other large grabens within the map area first before considering Red Lake Canyon.

Red Lake Canyon is the main stream channel of the only integrated through-going drainage within the north end of the graben system. During heavy precipitation it receives the runoff from the Butler Wash and Chesler Canyon drainage basins (Fig. 1) together with some runoff from Cyclone Canyon, and carries the flow to Lower Red Lake Canyon. The rapid deposition of sediment load in Red Lake Canyon, due to its gentle north-sloping floor, has resulted in the accumulation of a thick blanket of alluvium. The floor is criss-crossed by numerous braided channels, some up to tens of meters wide. The alluvium in places overlaps and partially buries the talus prisms along the walls of the canyon, indicating that the sediment accumulation has proceeded faster than the growth of the talus.

A reconstruction of the integrated prefaulting drainage, based in part on the remnants of this drainage preserved on the intergraben divides, shows that Red Lake Canyon also must have been a major component in that drainage network (McGill and Stromquist, 1974, Fig. 27). A paleogeographic reconstruction might show Red Lake Canyon as a broad stream valley incised along the N15-30E joint direction. Thus, during subsequent extension in the direction of regional dip, Red Lake Canyon would have been a favorably oriented zone of weakness. Initial failure, preceding early graben development, probably occurred in the rocks beneath the canyon floor.

As compared to other grabens, the scarps along the Red Lake Canyon graben are very irregular and marked by discontinuities, particularly south of the head of Lower Red Lake Canyon. Several large inward-rotated joint block rows are present along the margins of the graben. One of these (Fig. 4, loc. 8) is shown on section A-A'. A second example, similar to that in Unnamed Canyon, is illustrated diagrammatically on a cross section 900 m north of section A-A' (Fig. 4, loc. 9; Fig. 10). In addition, large talus prisms present along much of the length of the canyon indicate extensive collapse which destroyed any vestige of the original fault scarps. The original faults, as shown on the geologic map, are inferred to be buried beneath the talus.

The structure at the north end of the graben is somewhat less complex. The faults converge along strike to a minimum separation of about 75 m as displacement dies out northward. The east fault scarp along the north end of the graben shows a sharp sawtooth pattern similar to the Lens Canyon faults (Fig. 4, loc. 10). In this case, the fault scarp moves progressively westward along successive N15-30E joints in left en-echelon arrangement. The inferred subsurface shape of the faults in the north end of the canyon is that of a blunt-ended canoe.

Cyclone Canyon graben. The portion of the Cyclone Canyon graben that lies within the map area is 380 m wide and about 100 m deep. Both faults maintain a uniform N25-30E trend and here, as elsewhere, the dips of the faults at the surface are vertical. The floor is nearly flat and covered by alluvial and eolian deposits. Talus has accumulated along the base of the fault scarps, but is generally contained within 50 m of the scarp, suggesting relatively slight secondary widening by collapse.

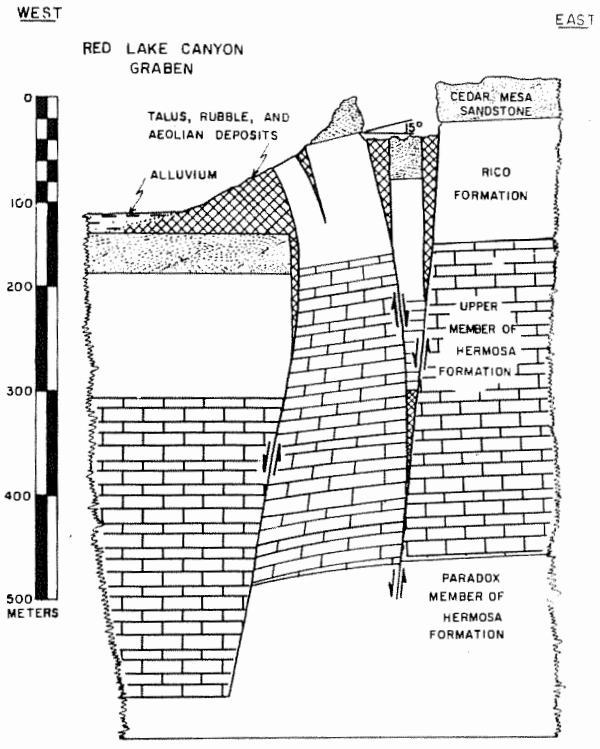

Figure 10: Structure of a collapsed joint block row on the east side of Red Lake Canyon. The subsurface geometry is inferred from the topography, shown accurately in this illustration, and the structure of exposed bedrock. Small keystone blocks, as shown here behind the inward rotated block, are characteristic of the secondary structure in large, complex grabens.

- -

An inward-rotated joint block row in an early stage of collapse is present along the east fault within the map area (Fig. 4, loc. 11). The overall geometry is relatively simple in comparison to other grabens described above.

Structure of the Intergraben Divides

The intergraben divides are characterized by an erosional surface of generally low relief broken by two sets of open joints, by small grabens with generally minor areal extent, and by remnants of an integrated prefaulting drainage. The dip of the intergraben divides commonly reflects the 3° to 4° northwest regional dip. The dip rarely exceeds 5°, except along Cataract Canyon and near Lower Red Lake Canyon where steeper dips are encountered. The width of most intergraben divides is about 750 m and is rarely less than 500 m, suggesting systematic spacing of grabens.

Reversal of the regional dip along the southeast side of Cataract Canyon has formed a subtle, broad syncline within the map area that trends nearly parallel to the strike of the grabens. The west flank of this syncline corresponds to the east limb of the Meander anticline south of the confluence of the Green and Colorado Rivers. The east flank of the syncline is the gentle regional dip. Between Lower Red Lake Canyon and the Chesler Canyon lineament, the axial trace of the syncline is located approximately between Red Lake Canyon and Twin Canyon. Farther north the axial trace is located near the east side of Red Lake Canyon. The structure dies out northward south of the Elephant Canyon drainage (Fig. 1) as a result of a change in the direction of regional dip. The syncline is clearly shown on cross section A-A' (Plate 2).

Plate 2 demonstrates that there is no significant structural relief between adjacent intergraben divides because the projection of bedding contacts across grabens would yield a smooth, continuous surface. This

relationship is generally true except near Cataract Canyon and in the vicinity of Lower Red Lake Canyon, where complex relative displacements among intergraben divides are common.

Anomalous uplift and tilting of the divides on either side of Lens Canyon have already been described. Two additional anomalous structures were observed within the map area: (1) relative uplift of the north end of the Twin Canyon-Unnamed Canyon intergraben divide and general south to southwest tilting of this block, and (2) relative uplift and general southeast tilting of the narrow divide between the north end of Twin Canyon and Lower Red Lake Canyon. The form of uplift and tilting in these two areas combined with the broad northeast tilting of the Lens Canyon-Red Lake Canyon divide suggest that the prefaulting structure in this local area might have been a broad uplift, about 2 km in diameter, roughly centered around the right-angle bend in the floor of Lower Red Lake Canyon south of Lens Canyon (Fig. 4, loc. 12). The complexities at the ends of the various grabens exposed on the walls of Lower Red Lake Canyon, may be due both to the presence of Lower Red Lake Canyon as an internal boundary and to partial collapse of this uplift when subsurface movement of evaporites into Cataract Canyon began.

Structural analysis of the intergraben divides must consider the nature and arrangement of minor faults mapped on the surface of the divides as well as the spatial orientation of the divides as major structural units. Minor faulting in the interior regions of the divides, characterized by en-echelon normal faults with less than 3 m of displacement and by small grabens formed near the rims of transverse drainages, is distinguished from minor faulting along the margins of grabens

associated with inward rotation and collapse of joint-bounded blocks. The latter has been described as a process of secondary graben widening and is included in the structural framework of large grabens. For the purpose of this report the distinction between the two categories of minor faults is made on the basis of kinematic differences in their origin.

Several small grabens were mapped on the Red Lake Canyon-Cyclone Canyon divide in the southeast corner of the map area (Fig. 4, loc. 13). These structures vary in width from 30 to 75 m and in depth from 0 to 10 m. Faulting is locally confined to the rim of transverse drainages and dies out rapidly along strike. In general, the faults conform to single master joints in the Cedar Mesa Sandstone. The southernmost of these grabens extends for about 1 km southwest from its origin on the south wall of the cross drainage (Fig. 4, loc. 14). It widens and deepens rapidly southward to form a right en-echelon continuation of Cyclone Canyon. The fault scarps display a sawtooth pattern, thereby establishing this graben as a possible kinematic analog of larger grabens.

Two small grabens have formed on the south wall of Lower Red Lake Canyon between Twin Canyon and Unnamed Canyon (Fig. 11). Over 30 m of displacement were measured on the east and west faults of the easternmost graben near the rim of Lower Red Lake Canyon (Fig. 4, loc. 15). The faults dip vertically to a depth of 100 m, then converge northward and downward to intersect at marker h. Dips of 84° and 86° were measured on the east and west faults respectively below 100 m. The east fault continues northward with displacement of about 25 m down on

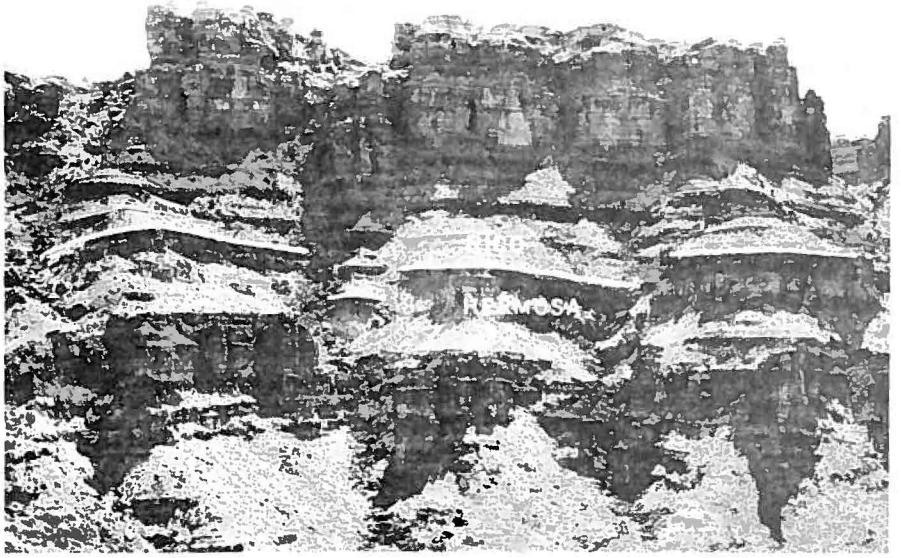

Figure 11: Two small grabens exposed on the south wall of Lower Red Lake Canyon. The faults bounding the small graben on the left clearly converge downward with average dips of 85°. The graben on the right is less distinct, but the faults may be seen to die out upward on the canyon wall. The Rico-Hermosa contact is highlighted to emphasize the structure.

- -

the west, but dies out before reaching the canyon floor. This graben extends only 250 m south from the rim of Lower Red Lake Canyon and dies out southward along north-dipping ramps.

Faulting associated with the second of the two small grabens is confined mostly to the Hermosa (Fig. 4, loc. 16). The principal bounding faults are separated by 30 m at marker unit h and converge downward and northward in the Hermosa. The westernmost fault dips 82° east and displaces marker unit h 10 m down to the east. The fault dies out upward and southward as a drag fold, and beds above marker d show no displacement. Displacement on the easternmost fault is 11 m down on

the west, measured on unit h, and similarly dies out up section such that beds above marker e are unfaulted. It is suggested that this structure is analogous to the small graben described above, but in an earlier stage of growth and, therefore, demonstrates initiation of faulting in the subsurface and propagation of faults upward and along strike.

Minor faulting is also present on the Red Lake Canyon-Lens Canyon divide. A series of left en-echelon normal faults strike subparallel to and approach the east fault of Lens Canyon (Fig. 4, loc. 17). The faults have a consistent west-side-down displacement sense, except where the structure dies out southward as a small graben.

Mechanical Analysis of Faulting.

Although data on the strength of the sedimentary rocks overlying the Paradox Member are not available, it is still possible to relate the observed geometry of the faults in the study area to laboratory data on the failure of triaxial test specimens of similar materials. To do this it is necessary to make some assumptions about the kinds of stresses and the intensity of stresses acting on these rocks when faulting was initiated. Hereafter, the term brittle plate will be used to describe the rock units above the Paradox Member.

Two elements of the geometry of graben faults in cross section were found to be consistent throughout the field area: (1) the fault scarps are vertical to a depth of 100 m, corresponding to the thickness of the uneroded Cedar Mesa Sandstone and that part of the Rico Formation above market unit d, and (2) below marker d average fault dips measured in Lower Red Lake Canyon are greater than 75° but are clearly less than

90°. Where bedding planes are principal planes, the assumption that the faults are shears which developed in isotropic rocks requires an angle of internal friction greater than 60°, if the Mohr-Coulomb criterion is applied uncritically. But application of the Mohr-Coulomb criterion to the dipping segments of faults is difficult, because the rocks are highly anisotropic due to both bedding and pervasive jointing.

Fault dips were not measured on outcrop, but instead were measured by lining up on strike with the fault scarp and measuring the dip of the fault trace on the wall of Lower Red Lake Canyon. These measurements yield average dips for large segments of the faults. At closer range, the fault is seen in detail to be a step-like succession of vertical segments connected by segments dipping between 65° and 70°. This suggests a strength inhomogeneity caused by rock units with low cohesive strength that fail on shear planes at angles between 20° and 25° to the maximum principal stress (oriented close to vertical due to gravity), and units with high cohesive strength that fail by slipping along preexisting vertical fractures. In order to assign a range of values of cohesive strength, it is helpful to develop a simple stress model to investigate the stresses acting on a portion of the brittle plate at failure.

Figure 12 is an idealized cross section in the vicinity of Cataract Canyon illustrating the probable effect of prefaulting evaporite flow on the structure of the brittle plate. The assumed configuration of stresses is shown on the right-hand side of the section. The coordinate system is defined with x parallel to bedding and in the direction of dip and y

perpendicular to bedding. The stresses at any point in two dimensions due to the weight of overburden are:

$$\sigma_y = \rho g y \text{ (compressive stress positive)}$$

$$\sigma_x = \frac{v}{1-v} \sigma_y \text{ (Hafner, 1951, p. 380).}$$

where v is Poisson's ratio taken as .20 to .33 for most geological materials (Price, 1967, p. 8). Although lithostatic stresses strictly

- -

Figure 12: Idealized prefaulting cross section through Cataract Canyon and an adjacent segment of the north end of the graben complex, illustrating possible boundary stresses (after McGill and Stromquist, 1974, Fig. 7). Accelerated canyon cutting in Recent time permitted flow of evaporites (heavy arrows) down the westward regional dip and upward beneath the river bed. Flow from the west, opposed to the regional dip, was confined to a narrow zone adjacent to the canyon. Accumulation of evaporites beneath the Colorado River and its deeper tributaries, occurring locally as dome-like intrusions (Fig. 7), caused arching of the rocks overlying the Paradox Member, creating the Meander anticline and the Lower Red Lake Canyon anticline (Fig. 6). Extrusion flow would superpose shear stress, τ_{xy}, on the base of the overlying sedimentary rocks. A supplementary tensile stress, $\sigma_{x(2)}$, due to the component of weight acting parallel to the regional dip (x coordinate direction) and approximately uniform with depth, is a consequence of updip attachment to strata outside the domain of subsurface flow. This component of body force is distributed over the lowermost 360 m of the brittle sedimentary rocks because open master joints in the uppermost 100 m prohibit these rocks from transmitting tensile stress parallel to bedding. Vertical and horizontal lithostatic stresses, σ_y and $\sigma_{x(1)}$ respectively, are shown acting perpendicular and parallel to bedding. This is a reasonable approximation because of the low ($\sim$4°) regional dip. The inset (upper right) shows the total stress acting on an infinitesimal free body in the x-y plane. Leaders from the inset to 100 m and 460 m depths designate the stratigraphic locations for analyses of total stress in Figure 14. It is assumed that subsequent faulting will occur near the right-hand side of the cross section.

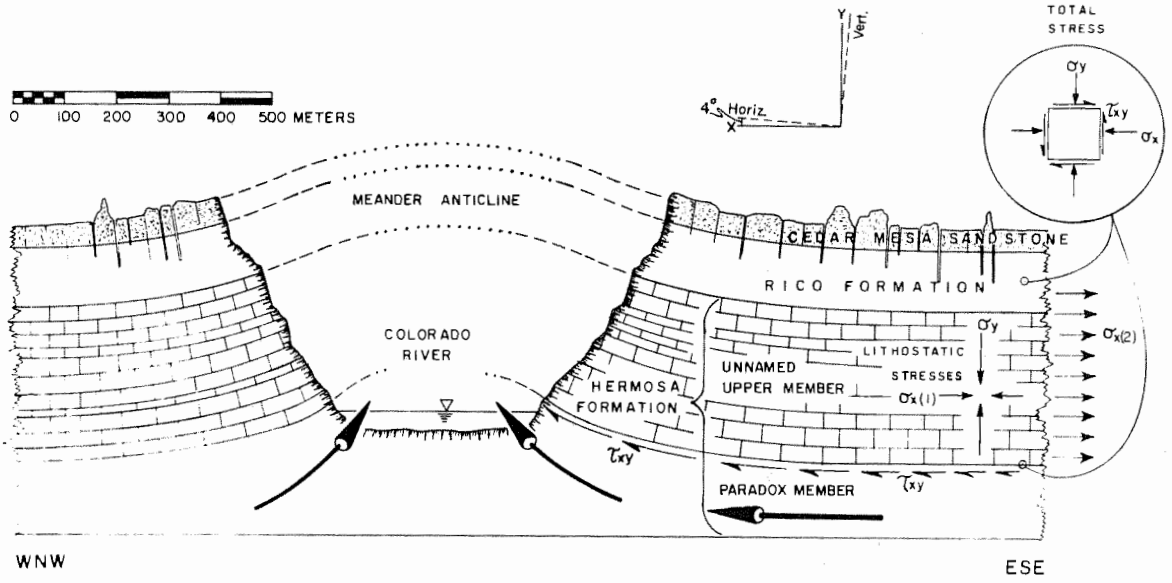

act in the vertical and horizontal directions, the error in magnitude introduced by assuming that these stresses act parallel to the x and y directions is considered negligible because the angle of dip is small. By assuming plane strain (Timoshenko and Goodier, 1955, p. 12), the components of shear stress acting on planes perpendicular to the x-y plane are zero; and σ_z, the component of stress normal to the x-y plane, is a function of σ_x and σ_y. Thus, the stresses in the x-y plane are functions of x and y only.

Two supplementary stress systems are superposed on the lithostatic stresses. The first is a tensile stress, $\sigma_{x(2)}$, due to the component of body force acting parallel to the dip of bedding. The need for this

stress is justified by likening the brittle plate to a block resting on an inclined plane and attached at the top of the plane. In the case where no flow occurs within the Paradox Member, this stress is approximately compensated by frictional resistance along the base of the block. On the other hand, where evaporites are flowing beneath the brittle plate, the inclined plane can be considered frictionless (in the extreme case), permitting $\sigma_{x(2)}$ to attain its maximum magnitude.

The second supplementary stress is due to the viscous drag exerted by evaporite flow. This viscous drag superposes a shear stress, τ_{xy}, acting parallel to the base of the plate in the direction of flow, which decreases in magnitude upward.

The first of these supplementary stresses, $\sigma_{x(2)}$, is proportional to the width of the brittle plate in the dip direction and is therefore a direct function of x. The second, τ_{xy}, is proportional to the equivalent viscosity and flow velocity of the evaporites. Because the rate of flow decreases to zero at some point updip and the magnitude of the shear stress must decrease upsection to zero at the earth's surface, τ_{xy} is a complex function of x and y. Since it is beyond the scope of this analysis to determine the form of this function, it is sufficient to recognize that the total shear stress due to viscous drag acting on a segment of the brittle plate is the integral of τ_{xy} over the width of this segment. Thus, at the base of the plate, the superposed shear stress is also a function of x only.

It is a simple matter to determine the lithostatic stress at any point by choosing 2.60 c.g.s. as the average value of density of the brittle plate and .20 to .33 as minimum and maximum values of Poisson's

ratio, thereby defining a range of $\sigma_{x(1)}$ from 1/4 to 1/2 of σ_y. The magnitude of the supplementary tensile stress can be estimated using the same value of density and selecting 460 m as the thickness of the brittle plate and 4° as the regional dip. The component of body force parallel to the regional dip is assumed to be carried by the lower 360 m of the brittle plate because open master joints in the uppermost 100 m prohibit these rocks from transmitting tensile stress parallel to bedding. As a first approximation, it is assumed that the stress is uniform with depth and that individual beds transmit equal tensile stress.

Possible magnitudes of the supplementary shear stress can be deduced in a qualitative way from field observations and results of triaxial tests on brittle sedimentary rocks.

Handin presents data on crushing strength, cohesive strength, and internal friction for sedimentary rocks from triaxial tests at room temperature and low confining pressure (Handin, 1966, Table 11-4). The data are mostly for Upper Paleozoic and Mesozoic rocks from various localities. The data are summarized in Figure 13 as two sets of failure envelopes representing average upper and lower values of τ_o and the average range of internal friction. To a first approximation, this range is taken as representative of the rocks in the field area.

Figure 13 illustrates the results of analyses of total stress at 100 m depth and 460 m depth. The analysis at 100 m depth places some limits on the tensile strength of the brittle plate. The fact that rocks in the uppermost 100 m are capable of supporting a vertical fracture to a maximum depth of 100 m suggests that failure in this zone was strictly tensile and took the form of separation along old master

joints. The extreme effect of pervasive fractures oriented perpendicular to the extension direction would be to reduce the overall

- -

Figure 13: Summary of cohesive strength and internal friction for sedimentary rocks from triaxial tests at low confining pressure and room temperature. An average range of failure envelopes (dashed lines) is shown for average high and low values of cohesive strength, τ_o, designated as strong and weak, respectively. The superposed horizontal tension, $\sigma_{(x)2}$, increases at the rate of about 2.3 bars per 100 m in the direction of dip, assuming an average density of 2.60 gm/cm^3 and a dip of 4°. The magnitude of this stress was computed using the average distance between the centerlines of adjacent grabens, 1000 m, as the updip distance to the next zone of failure. The Mohr circles for total stress at 100 m depth (small circles) were constructed for end member values of Poisson's ratio, v, of .20 and .33. Since master joints are closed at depths greater than 100 m, a range of overall tensile strength between 11 and 17 bars is suggested. On this basis a range of failure envelopes in the tensile region (dotted curves) is illustrated for strong rocks. Similarly, Mohr circles were constructed for total stress at 460 m (large circles). It is shown that when the stress function τ_{xy} is zero, strong rocks (v = .20) will not fail either in shear or in tension. Simple manipulation of the Mohr circle for v = .20 will show that τ_{xy} must reach a magnitude of at least 45 bars to permit tensile failure in rocks with high cohesive strength. Similarly, for the larger value of v, τ_{xy} must have a total magnitude of about 46 bars to permit shear failure of weak rocks. As a result of this shear stress, σ_1 would be inclined about 25° to the vertical, making the conjugate graben faults asymmetric with respect to vertical. The observed lateral symmetry of Canyonlands grabens requires that σ_1 remain close to vertical. But if the superposed shear stress were to die out rapidly upward, the resulting asymmetry in the lowermost beds would never be observed in the field, because these rocks are not exposed directly beneath grabens. By extending this analysis to depths between 100 and 460 m it is possible to calculate an approximate minimum total stress necessary to produce failure of both strong and weak rocks at any intermediate depth.

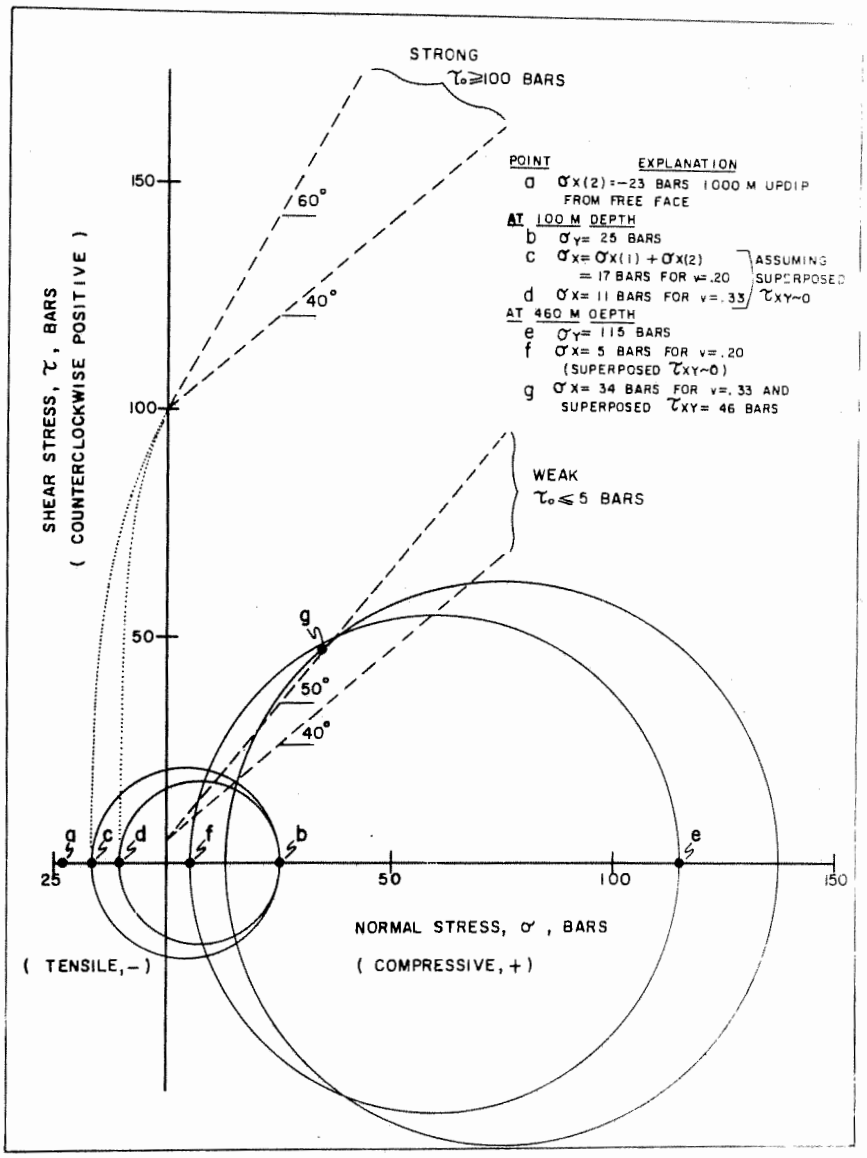

tensile strength to zero. The observation that tensile fractures are closed below 100 m suggests that the brittle plate possesses cohesive strength and therefore finite tensile strength. Figure 13 shows a range of tensile strength from 11 to 17 bars depending on the choice of

Poisson's ratio. Based upon the range of internal friction shown for weak rocks, it is inferred that the lowest permissible value of τ_o in the upper 100 m is about 18 bars, but that τ_o probably exceeded 26 bars.

The analysis of total stress at 460 m depth provides a means for estimating the magnitude of the supplementary stress, τ_{xy}. Figure 13 shows that τ_{xy} must reach a magnitude of 46 bars for Poisson's ratio of .33 to permit weak beds with the steeper of the two envelopes to fail in shear. For strong rocks, τ_{xy} is necessary to make σ_x negative, thereby permitting tensile failure. It can be shown with Figure 13 that τ_{xy} must be at least 45 bars in order to exceed the minimum tensile strength determined above. In this stress state the maximum principal stress would be rotated 25° from vertical in the downstream direction and asymmetric grabens would be expected. However, strong lateral symmetry characterizes Canyonlands grabens and seems to require that σ_1 remain close to vertical at any depth. A strong fault asymmetry could develop in the lowermost beds of the brittle plate if the shear stress died out rapidly upsection, but such an asymmetry could never be observed in the field because there are no exposures of the base of the brittle plate directly beneath a graben. It is considered unlikely that a large τ_{xy} would decay to a negligible value in such a short distance upsection. For this reason the magnitude of τ_{xy} is limited to a few tens of bars.

The net effect of τ_{xy} and $\sigma_{(x)2}$ is to increase the stress difference $(\sigma_1-\sigma_3)$ so that the Mohr circle for the combined state of stress intersects the failure envelope for weak beds or exceeds the tensile strength for strong beds. This allows two modes of failure to occur, depending on the cohesive strength of the rocks. Those with low

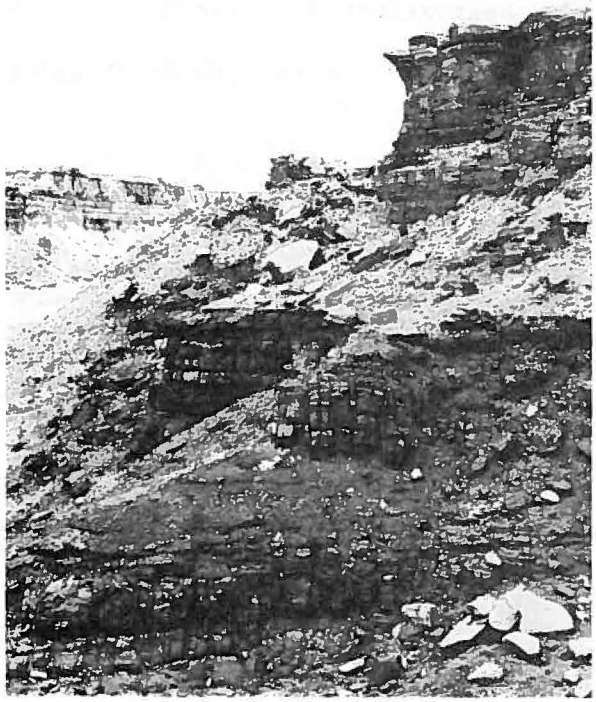

Figure 14: Normal faulting along preexisting fractures as seen on the east wall of Red Lake Canyon.

- -

values of τ_o for which failure envelopes fall within the Mohr circle will fail in shear on planes at 25° to 30° to σ_1 (Fig. 13), whereas those with larger values of τ_o, 100 bars for example, will fail by slip along old fractures (Fig. 14).

Even though this analysis does not consider all the possible variations in the state of stress, it resolves the observed dip of the faults in terms of the physical properties of the rocks and the approximate magnitudes of the stresses attendant upon failure. Furthermore,

this analysis has offered well-founded arguments to suggest that the brittle rocks cannot support vertical faults to the depth of the flowing layer. Indeed, observations in Lower Red Lake Canyon have established that overall fault dips decrease with depth and that graben faults are convergent downward.

Flow in the Paradox Member

Loss of confining pressure on the evaporites with canyon cutting would give rise to a steep local pressure gradient within the Paradox Member beneath Cataract Canyon. Initially, evaporites would extrude from beneath the brittle plate into the region of low pressure. In this phase of flow, the maximum velocity in the flowing evaporite layer would occur at some depth below the brittle/ductile contact due to the effect of a boundary layer. Thus, shearing stress would be superposed on the base of the brittle plate by viscous drag. The sense of the shear stress is in the direction of flow (Fig. 12). It is suggested that failure of the brittle plate might be localized over a zone where the effect of the shear stress is greatest.

Following the separation of the brittle plate along the failure zone, the downdip segment of the plate would continue to move as a decollement. The sense of the superposed shear stress on the base of the detached block would be reversed, since viscous drag would act to resist gravity sliding. This scenario for continued translatory movement of the detached block as a decollement is suggested by Nye's analysis of the flow of a narrow valley glacier down a uniform slope (1952, p. 83). Nye's model applied to this phase of the deformation

would predict that the velocity of the evaporite layer reaches a maximum at the brittle/ ductile contact and decreases with depth. Hence, it is suggested that the detached block would move at the maximum velocity of the evaporites. At the same time, extrusion flow would continue updip beneath the intact portion of the brittle plate.

SIMULATION OF GRABENS WITH GEOLOGIC SCALE MODELS

Introduction

The purpose of using geologic scale models in this investigation is to determine whether, in fact, grabens do form according to Baker's hypothesis (1933), and, if so, to analyze the kinematics of graben growth and to identify the features that characterize the geometry. It is not intended that the results be applied in a direct quantitative way to predict the dynamic response of the rocks in the field area. Furthermore, no attempt will be made to justify the validity of the models in terms of the strict theory of scale modeling. Although Hubbert (1937) showed that fundamental model ratios can be specified for geologic processes without violating the principles of the theory, the objection is still often raised, and properly so, that since the strain rate and rheological properties at the time of deformation can never be known precisely, geologic scale models can never be more than an interpretive aid. Thus, the real value of demonstration models is their usefulness in testing hypotheses, observing processes, and eliminating erroneous interpretations. The following excerpt (Belousov, 1961, p. 97) puts the role of geologic scale models in proper perspective:

> Failing direct observation of the tectonic processes, some geologists have been finding that they can learn a great deal from scale models set up to simulate such processes in the laboratory. Experiments with these models yield no real proof but they do make it possible to see processes that can otherwise be visualized only in the mind's eye.

Demonstration models have been used frequently to study the movement of evaporites that occurs at great depth in young sedimentary basins,

particularly in relation to the growth of salt diapirs. Some workers have examined the formation of fractures over salt domes and salt anticlines (Link, 1930; Nettleton and Elkins, 1947; Parker and McDowell, 1951, 1955; Tanner and Williams, 1968). Sanford (1959, p. 42-43) obtained horst and graben structures using dry sands and clays in a simulation of the response of homogeneous sedimentary layers to basement uplift. Cloos worked with sand and clay models to study the growth of faults, fractures, and peripheral grabens along the Gulf Coast (1968, p. 433-437). Several of Cloos' figures provided part of the inspiration for the scale-model phase of this investigation. Finally, McGill and Stromquist (1974, p. 44-52) reported the initial results of work with sand models to simulate the development of grabens by subsurface flow.

Methods

The object of this study is to investigate the response of a brittle layer to tensile stresses superposed by flow of an underlying plastic layer. Two modeling materials are required to simulate the rheology of the evaporite strata and the overlying brittle sediments. Paraffin wax was chosen for the former and unsorted kiln-dried sand for the latter. The use of granular substances to simulate the behavior of brittle rocks is well established (Nettleton and Elkins, 1947; Hubbert, 1951; Sanford, 1959; Cloos, 1968). Various combinations of sand and powdered materials were tried to find a mixture that would show visible fractures when deformed in layers several centimeters thick, but which were not so strong that they would support open tension gashes. A mixture of ten parts sand to one part finely ground limestone was selected. The results of a sieve test on the sand alone and of eleven

controlled-strain direct shear tests on the mixture are shown in Figure 15 and 16. The Mohr envelope in Figure 17 indicates an angle of internal friction of the mixture of 45°. This is an apparent value since the data were not corrected for normal strains. The mixture was found to have an average dry bulk density of 1.60 gm/cm^3. Ground limestone was also used separately to construct a smooth 1 to 2 mm surface over the sand layer. It served a dual purpose; as a cohesive material it supported vertical fractures similar to those in the Cedar Mesa Sandstone and at the same time it provided visual enhancement of the faults and fractures in the sand.

The household variety of paraffin wax was used for these experiments. The density was found to average between .55 and .60 gm/cm^3 at 25°C. Because paraffin is a poor heat absorber, it is a less than ideal modeling material for these experiments. The heat required to reduce the viscosity of a 1.5 cm layer so that it would deform plastically, produced severe melting at the base of the paraffin layer, particularly in the center of the model. A more uniform viscosity with depth and a sufficient reduction in melting at the glass/paraffin boundary was achieved by mixing powdered lamp black into the paraffin before molding. A thin film of molten paraffin at the glass surface was necessary to the operation of the models because the film served as a lubricant on which the cooler plastic paraffin stretched in response to overburden pressure from the sand. The early extrusion phase that has been postulated for flow of the Paradox Member was not observed in these experiments. This is consistent with the mechanism for subsurface flow, in that the occurrence of extrusion flow is basically a function of the cohesive

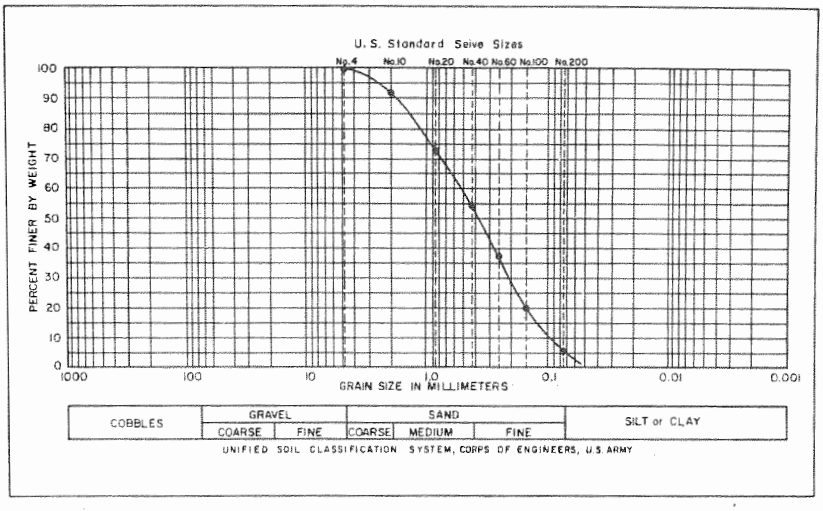

Figure 15: Grain size distribution of unsorted dry sand.

- -

strength of the overlying material and the viscosity of the flowing layer. Because the sand layer has almost no intrinsic strength, it failed after a small amount of strain in the paraffin layer.

An apparatus was designed and constructed on which controlled experiments could be performed (Fig. 17). It is a rigid steel structure with a plate glass top set in a 100 x 70 cm metal frame. The frame is hinged on one side so that the glass surface can be rotated to the desired initial dip. A sliding overhead camera mount is attached to a horizontal track so that overlapping vertical photographs can be taken. Rheostatically controlled infrared lamps are used to heat the paraffin and maintain its plasticity during an experiment.

Construction of the models began with molding and hardening of the paraffin layer within the frame. Next, the sand mixture was spread over

the paraffin to the desired depth and leveled. Leveling and smoothing were done the same way in each experiment to keep compaction reasonably constant. Finally, a thin (1 to 2 mm) layer of ground limestone was added onto the sand surface and rolled smooth. Black powder was used to construct marker lines on the powdered limestone layer parallel to the long dimension of the model. To operate the models, the table top was rotated to the desired angle (~4°) and the downdip confining side was removed. The paraffin was heated rapidly until the first extension fractures were visible in the ground limestone layer. The intensity of the heat lamps was then reduced to a level sufficient to maintain deformation. When the desired fault geometry was obtained, after about 2 hours, the lamps were extinguished and the paraffin hardened. The locations of the faults near the base of the sand layer were preserved by paraffin ridges to which the faults at the surface could be correlated.

Results

Two series of experiments were run in which the models were built in either a 40 x 50 cm frame or a 50 x 90 cm frame, with the short dimension parallel to the direction of flow in both cases. The effect of varying the thickness of both the paraffin layer and the sand layer was investigated for each series. Some of the better models were hardened with cellulose acetate after completion of the experiment and cut in cross section.

Figure 18 illustrates the initial surface of model 5090.14. The sequential development of this model is shown in Figure 19. The model was constructed with a 7-mm paraffin layer, a 30-mm sand layer, and a

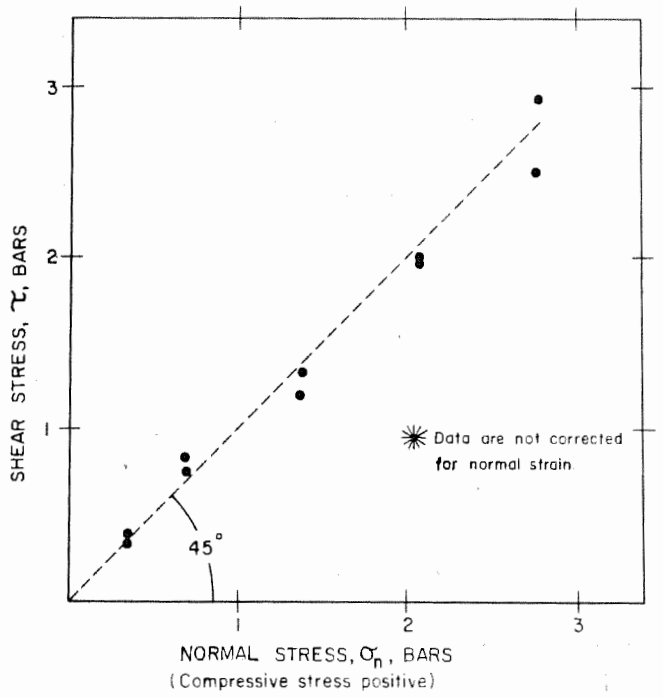

Figure 16: Controlled strain direct shear tests on a mixture of 10 parts dry sand to 1 part powdered limestone. The tests were performed in a shear box apparatus designed so that the lower half of a cylindrical sample cup is displaced laterally at a constant rate with respect to the fixed upper half. An infinitely variable normal stress is applied through a ram driven by a hydraulic bellows. Stress is determined by the elongation of calibrated prooving rings in each linkage. The tests were run at a nearly constant strain rate between 1.0 and 1.4 x 10^{-4}/sec.

- -

2-mm ground limestone surface in a 50 x 90 cm frame. The photographs cover a strip 40 cm wide in the center of the model. The sequential development of the single graben labeled I is of primary importance. Elapsed times are given with respect to the first recorded distortion of the black marker line closest to the unconfined edge.

Grabens first appear at the surface of the model as elongate downwarps between monoclinal flexures. The monoclines mark the subsequent position of the principal bounding faults. Initial displacement at the surface is by dip-slip motion along discrete preexisting fractures that belong to a set of early formed conjugate shears. With continued displacement, the individual faults coalesce into through-going parallel faults that clearly define the limits of the graben. Because the trend of the normal faults and the trends of the conjugate shear fractures are not parallel, the scarps along the grabens have developed a distinct sawtooth pattern. As in the case of Canyonlands grabens it is inferred that the faults originate at depth in the sand layer and propagate upward utilizing the preexisting conjugate shear fractures in the limestone layer. Because the faults develop simultaneously and approximately equal displacements occur on each fault, good lateral symmetry is maintained during the growth of the grabens. The faults remain parallel at the ends of grabens so that as displacement dies out the graben floors ramp up to the level of the unfaulted surface. In general, new grabens develop sequentially updip. Older grabens become deeper and wider and are modified by wall collapse and inward rotation of powdered limestone "blocks" bounded by early shear fractures. All in all, many similarities exist between the surface geometry of model grabens and that of Canyonlands grabens.

To understand the fracture geometry, it is necessary to define the boundary conditions within the model. The displacements, demonstrated by distortion of the black marker lines, are seen to decrease symmetrically from a maximum in the center of the model, to zero within 20 to

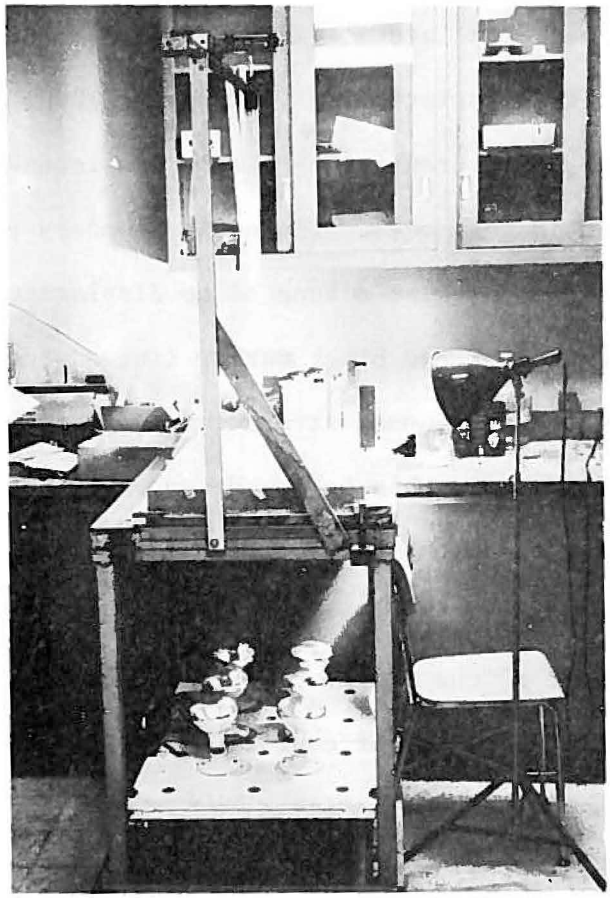

Figure 17: Apparatus used to perform scale-model experiments. The glass table top measures approximately 70 x 100 cm. A 50 x 90 cm frame for containing the paraffin, sand, and powdered limestone rests on the glass surface. Hinges on the left side and threaded bolts on the right side allow the table top to be rotated to the desired dip angle. The board supporting the infrared lamps is also hinged and can be swung upward so that photographs of the flowing layer can be taken through the glass surface with the camera on a second mount below (not shown). The floodlight provides low angle illumination.

- -

25 cm toward each side. This is the effect of a smooth temperature variation in the paraffin from ambient near the sides to about 50°C at the center. Because the viscosity of the paraffin is largely a function

of temperature, the lateral variation in displacement reflects a corresponding inverse variation in viscosity. Thus, the lateral boundaries are zones of rapid transition to zero displacement and are contained entirely within the model. The updip boundary parallel to the black marker lines is likewise a zone of no displacement, demonstrated by very minor distortion of the black marker line adjacent to the scale. Along the center line the normal strain rate is approximately constant, on the order of 10^{-2}/sec in this case. Hence, displacement within the paraffin varies from none at the updip edge to a maximum at the unconfined edge. Thus the boundaries that determine the areal extent of faulting are an intrinsic part of the model. The metal frame serves only to contain the model materials, except of course, along the free face, and imposes no constraints on the deformation.

Initially, the only stresses acting on the model are due to gravity. In this stress system, σ_1 is everywhere vertical and approximately normal to the surface of the model. Early displacement of the paraffin is accompanied by the appearance of vertically dipping conjugate shear fractures in the ground limestone layer (Fig. 19a). The acute bisector between any conjugate pair is known to be the orientation of the maximum compressive stress, σ_1 (Anderson, 1951, p. 14). Thus, by constructing the acute bisector at each intersection of shear fractures, the σ_1 and σ_3 trajectories can be mapped on photographs of the model (Fig. 21a). McGill and Stromquist (1974, Fig. 44) showed from results of an earlier series of experiments that while σ_1 trajectories become parallel to the surface at least within the powdered limestone layer, at some depth in the sand σ_1 is still vertical. At this level, σ_2 trajectories must

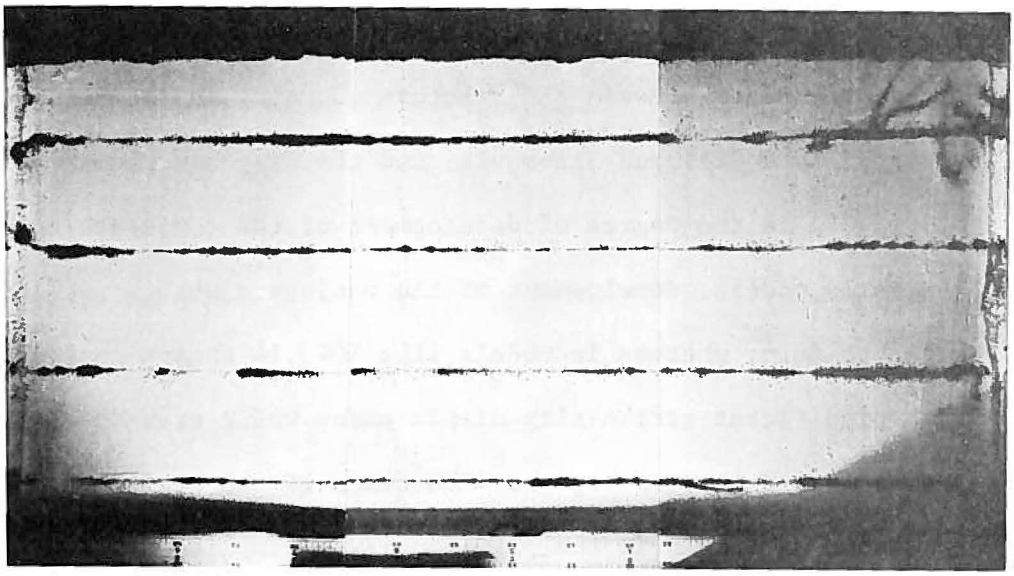

Figure 18: Composite vertical photograph of the initial surface of experiment 5090.14. The unconfined edge is at the top of the photo. Black marker lines on the powdered limestone surface are a mixture of lampblack and powdered limestone. The marker lines show subsequent downslope movement of the sand layer. The scale in the photo is labelled in centimeters.

- -

conform to the trend of the normal faults initiated at depth. Trajectories of minimum principal stress, σ_3, remain parallel to the surface and to the extension direction. Once initiated, normal faults can continue to propagate toward the surface, even though the maximum principal stress is horizontal within a near-surface layer. The traces of the faults at the surface, describing σ_2 trajectories at depth, are approximately parallel to the early near-surface σ_1 trajectories associated with conjugate shear development.

The pattern of faults and extension fractures formed in an advanced stage of deformation (Fig. 19d), may be used to infer σ_2 and σ_3 stress

trajectories at depth in an early stage of deformation (Fig. 21b). A major difference between the fracture geometry in the early experiments reported by McGill and Stromquist and the fracture geometry in model 5090.14 is in the degree of development of the conjugate shears. In the early models, development of the conjugate shears declined as grabens began to form, whereas in models like 5090.14 shears continue to develop with significant strike-slip displacement while grabens are forming in the central extending region. The trace of the strike-slip faults preserved as ridges in the paraffin layer, implies that σ_1 is approximately horizontal near the lateral margins of the moving portion of the

- -

Figure 19: Sequential development of model 5090.14.

a. After 18 minutes conjugate shear fractures have formed at the surface in the central part of the model and simple extension fractures appear adjacent to the unconfined edge.

b. After 21 minutes graben I appears as a synclinal trough between two monoclinal flexure zones. The zones are marked by a series of discrete normal faults (loc. 1 and 2) and inward rotated blocks (loc. 3 and 4) representing incipient dip-slip motion on the shear planes.

c. At 23 minutes the discrete faults have coalesced into well-defined through-going faults with strong sawtooth geometry (loc. 5 and 6). At this instant the graben is 2 mm deep.

d. After 27 minutes the depth has increased to 4 mm and the fault scarps have been modified by collapse (loc. 7) and rotation of fracture-bounded "blocks" into the graben (loc. 8). No significant lengthening of graben I has occurred.

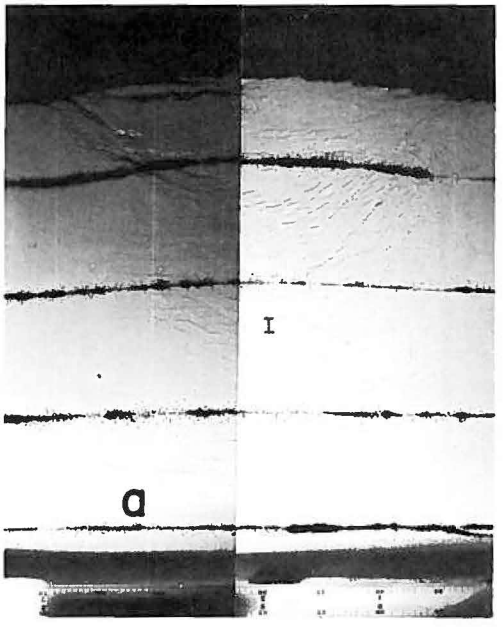
I
a

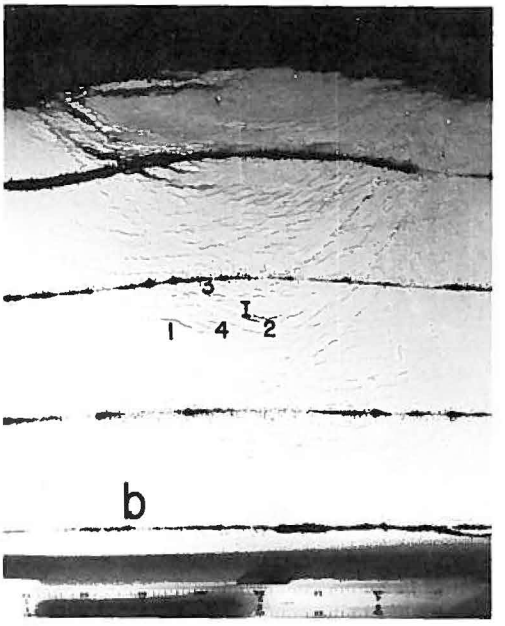
3
I
1
4
2
b

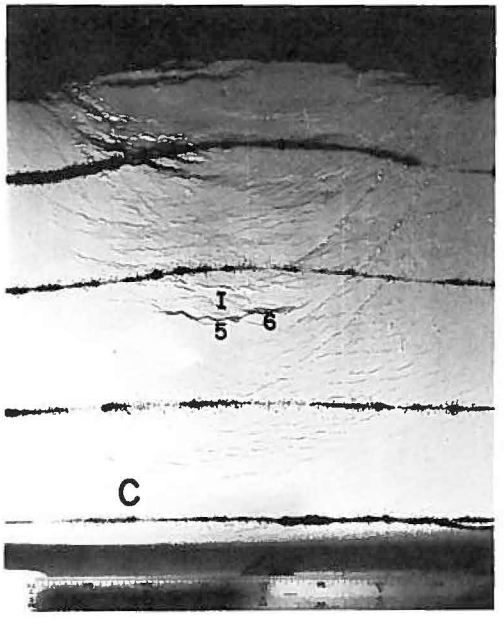
I
5
6
c

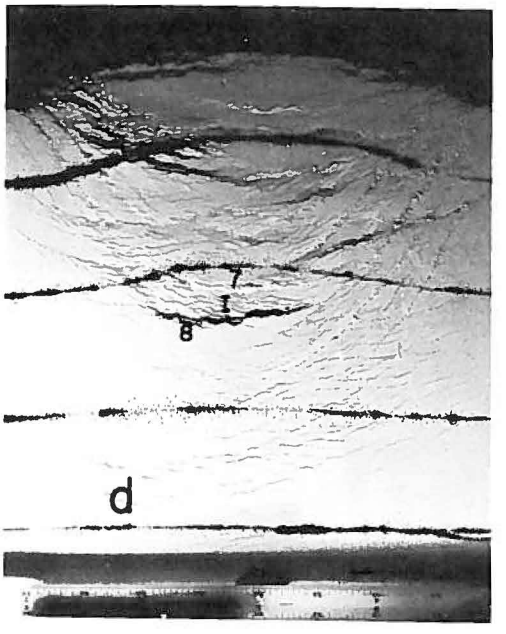
7
I
8
d

model through the total depth of the sand layer. Continued development of the shears in later models is attributed to changes made in the model apparatus. As a result of these changes the relatively simple fracture geometry developed in early experiments could not be reproduced.

The complex stress history of the model is underscored when Figure 20 is viewed stereoscopically. Continued deformation along the conjugate shears is evidenced by "brecciated" limestone powder and offsets of the black markers. In addition, motion along the shears may have a dip component or may be entirely dip slip.

McGill and Stromquist (1974, Fig. 43) have applied a stress model for a valley glacier in extending flow (Nye, 1952) to account for the curvature of the σ_2 stress trajectories in the experiments and, by analogy, to account for the curvature of the Canyonlands graben system. In Nye's stress model (Fig. 22), shear couples exist parallel to the direction of flow as an effect of lateral boundaries on the extending region and vary in magnitude from zero along a vertical plane containing the center line of flow to a maximum at the boundary.

The boundaries can take one of at least three possible forms. In the case of a valley glacier the boundary represents a change in shape of the flow channel, and the magnitude of the shear stress is a function of valley width, rate of flow, and the geometry of the wall to floor transition. In the experiments, the boundary takes the form of a lateral increase in viscosity of the flowing layer. Finally, in an earlier discussion (p. 21), the lateral boundaries of the Canyonlands graben system were inferred to represent a change in the geometry of the flowing layer. It is suggested that the mechanical boundaries in each case are

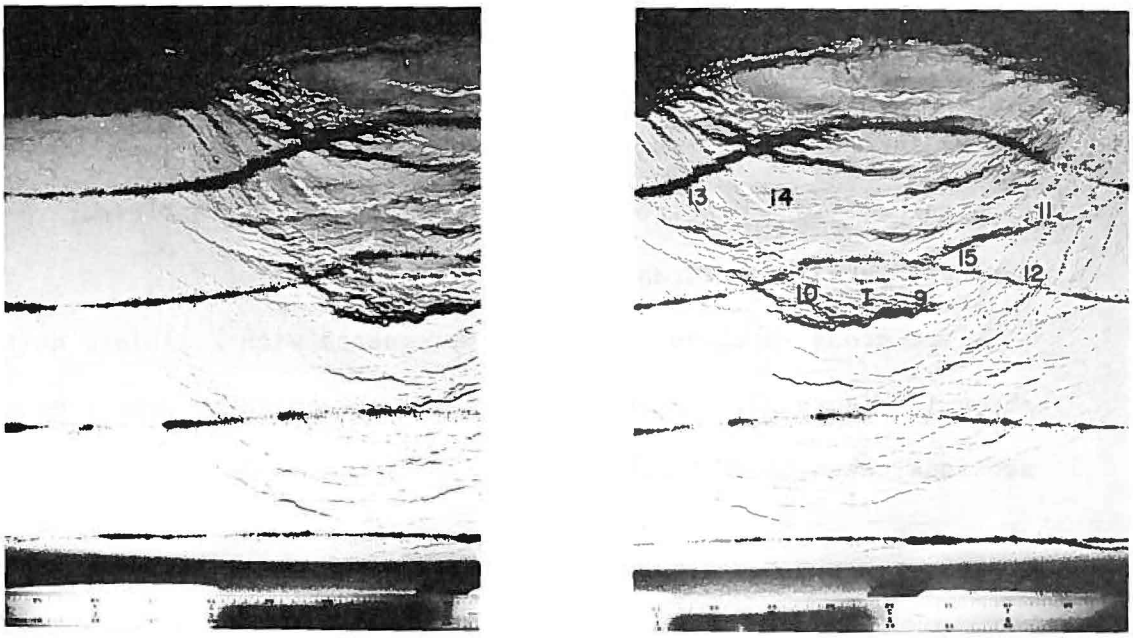

Figure 20: Stereopair of model 5090.14 at the completion of the experiment. A complex pattern of normal faults has broken the graben floor into smaller internal grabens (loc. 9 and 10) with features similar to those observed during growth of the larger grabens. Secondary widening occurs by inward rotation and collapse, while primary widening and deepening occur by fault separation due to additional extension.

analogous; they differ only in the detailed effect of the superposed shear stress on the reorientation of regional stresses.

Nye's (1965) model for glaciers in valleys of geologically reasonable shape, and the Canyonlands graben system are similar inasmuch as the transition from the extending region to the undeformed margins is so gradual that the effect of the superposed shear is only to reorient σ_2 trajectories. The lack of similarity with the experiments is attributed

to the abrupt lateral increase in viscosity of the paraffin layer. Here the effect of the superposed shear is both to reorient σ_2 trajectories and to interchange σ_1 and σ_2 near the margins where the superposed shear is greatest. The magnitude of the resulting σ_1 is sufficient to produce conjugate shear fractures seen in the brittle layer.

Two cross sections of models impregnated with cellulose acetate are shown in Figure 23. By assuming that plane strain is approximated along sections taken close to the center line of the model, the effect of the

- -

Figure 21: Stress trajectories during the formation of conjugate shear fractures. Dashed lines are principal stress trajectories. Dotted lines correspond to the black marker lines in Figure 19 and to the position of the unconfined face.

a. Maximum and minimum principal stresses in the powdered limestone layer. The solid lines making acute angles are conjugate shear fractures mapped on Figure 19a.

b. Intermediate and minimum principal stresses at some depth in the sand layer where σ_1 is still oriented approximately vertical due to gravity. The solid lines are normal faults mapped on Figure 19d. Hachures are on the downthrown side.

Figure 22: Stress model for a valley glacier in extending flow (Nye, 1952) simplified to show lateral distribution of shear stress in scale-model experiments. These shear stresses act on vertical planes striking parallel to the direction of flow. Stress intensity is shown in a qualitative way by the length of the arrows. Transverse shear couples, necessary to provide moment balance, are not shown in this model. Additional stresses not shown include lithostatic stress, a nearly uniform horizontal tensile stress tending to produce extending flow, and a smaller transverse tensile stress due to constant width.

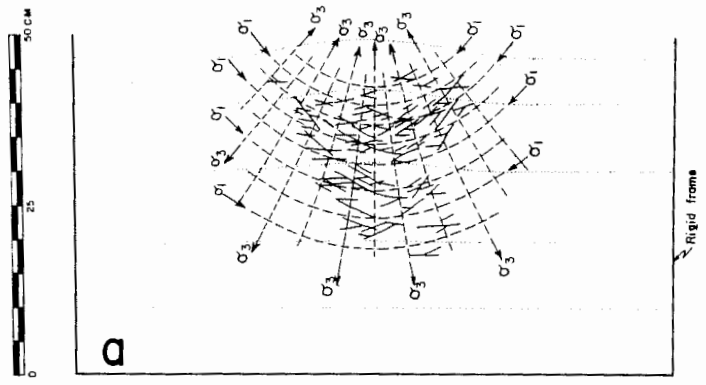
50 CM
25
0
Rigid frame
a

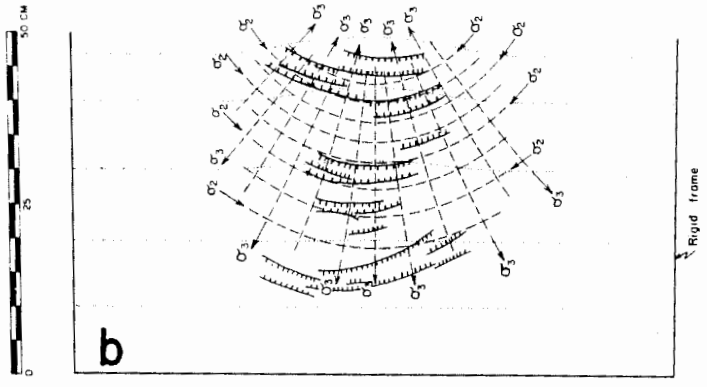
50 CM
25
0
Rigid frame
b

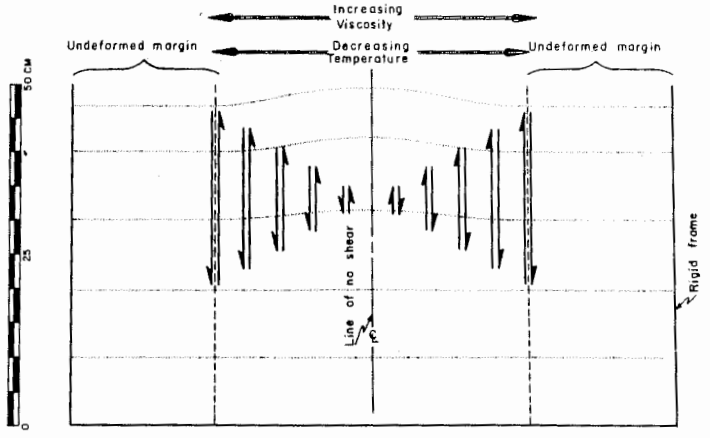
Increasing Viscosity
Undeformed margin
Decreasing Temperature
Undeformed margin
50 CM
25
0
Line of no shear
Rigid frame

conjugate shears can be neglected and the grabens viewed as if they had formed with prismatic geometry. This approximation is only valid in a general way since the curvature of the grabens is a result of the superposed shear stress. The conjugate fractures, once formed, exert their influence on the growth of graben faults.

Figure 23a illustrates a model that deformed so that the strain is approximately uniform along the line of section. Graben C is a major exception. Strain was initially concentrated along the trend of this graben, so that it grew nearly to the extent shown in the section before other grabens began to develop progressively updip and downdip. This sequence of growth is remarkably similar to the one proposed in a later section for the Red Lake Canyon area, except that there is no obvious reason why growth should have progressed this way in the model.

Several important features are illustrated in this cross section: (1) the grabens are clearly symmetrical, (2) the initial geometry of grabens in cross section is an isosceles triangle (A and B) with apex at the sand/paraffin contact, (3) the sand in the downfaulted graben blocks is redistributed to fill available voids created by fault separation and does not penetrate into the paraffin, and (4) the paraffin layer has thinned uniformly during flow.

Figure 23b illustrates a model in which the strain has been concentrated in three zones along which grabens have formed. It is distinguished from Figure 23a by marked thinning of the paraffin layer and the preferential growth of a few large grabens rather than numerous smaller grabens. The difference between the two models merely illustrates the difficulties in achieving reproducibility.

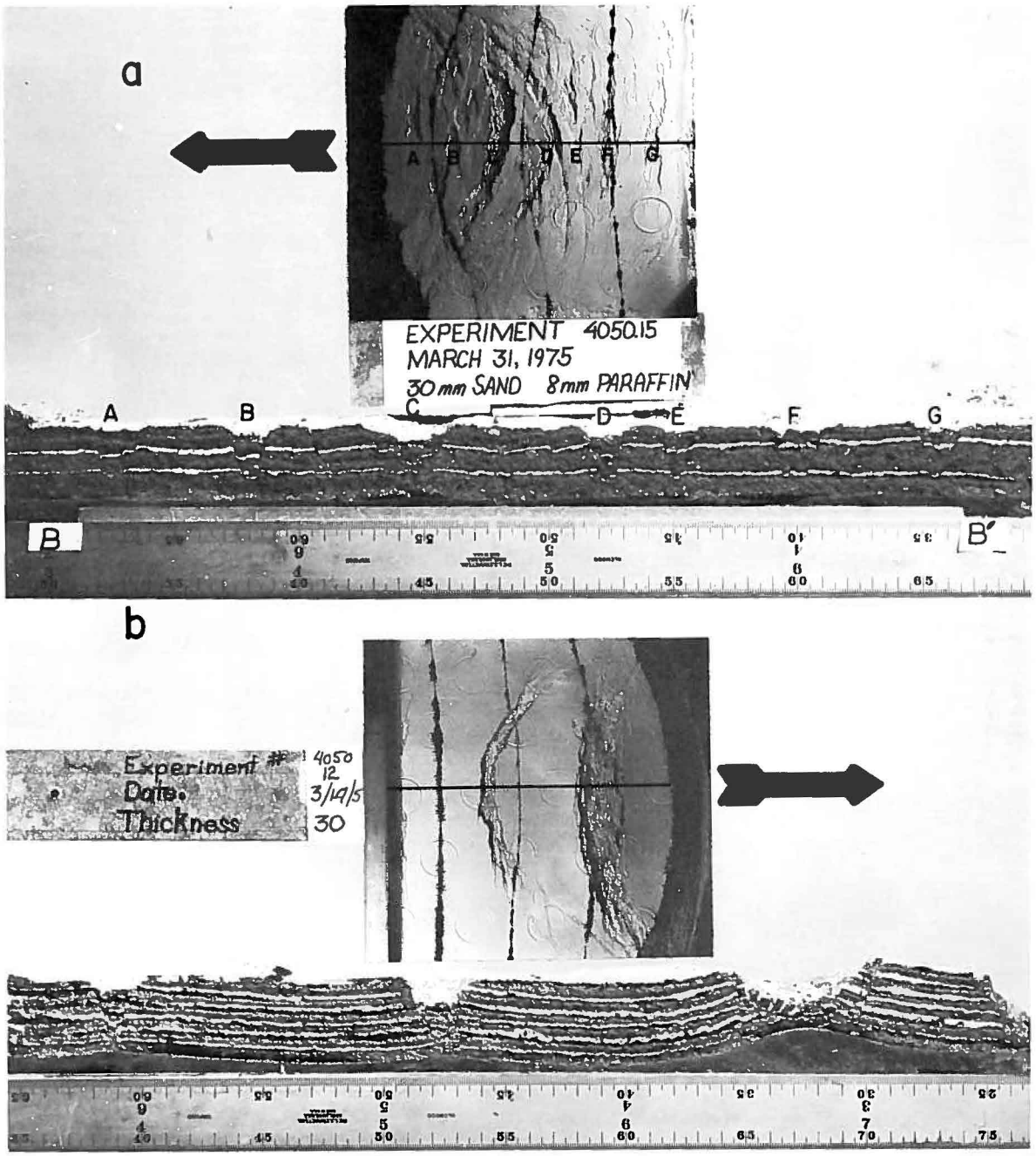

Figure 23: Cross sections of hardened models. Faults intersect at the sand/paraffin contact in the initial stage of graben development. Downthrown sand does not penetrate into the flowing layer. Paraffin ridges form beneath older grabens where the sand cover has been thinned by downfaulting and widening. Insets illustrate the surface of each model prior to hardening, and the location of the cross section. Arrows show the direction of flow.

Because of the many similarities in surface geometry between scale-model grabens and Canyonlands grabens, the geometric details shown by these cross sections may be used to suggest constraints on the subsurface geometry of the latter.

In Figure 23b the large graben on the right formed initially with geometry like the small graben on the left. Excessive widening and deepening of the former is a result of outward rotation of the early developed faults during the growth of the paraffin ridge. The white marker layers show a broad open anticline that is similar in many respects to the Meander anticline, even to the details of the downfaulted toreva blocks. An interesting question is raised by the geometric similarity between these two structures. If one were to imagine a stream flowing in the model graben that stripped away most of the downfaulted material to the level of the paraffin, then the origin of the remaining structure would be as problematical as the origin of the Meander anticline. Most geologists would interpret this kind of structure as the result of nonuniform loading of low density viscous strata; however, Tanner and Williams (1968, p. 13) observed that plasticity of the flowing layer may, in some cases, be more important than the density contrast between the flowing layer and the overburden in governing the movement of viscous materials into ridges and domes. The density contrast in Canyonlands is no more than .20, but each system responds in the same way. Knowledge of the extent to which each of these factors governed the flow of evaporites would bear strongly on the age of the Meander anticline and the timing of the Canyonlands grabens.

Summary of Model Simulation

About three dozen experiments were performed in which the effects of variations in the thickness of the sand layer and the paraffin layer were observed. It was found that a certain minimum thickness of paraffin and sand is necessary for deformation to occur. The paraffin would not creep under its own weight at normal operating temperatures but required a uniform overburden of sand at least 15 mm deep to drive it. Alternately, a model with over 15 mm of sand would not develop grabens if the paraffin layer was less than 5 mm thick. Beyond these minimum layer thicknesses the occurrence of grabens was not sensitive to the depth of the sand layer. The optimum dimensions of the models were 7 to 15 mm of paraffin and 30 mm of sand. For smaller total depths, keeping the ratio of sand to paraffin thickness constant, the grabens that formed were too small to work with. Models with greater total depth were too awkward to construct.

Figure 24 is a plot of the initial width of grabens as a function of depth of the sand layer. Despite scatter and the scarce data from models where sand thickness was greater or less than 30 mm, the data suggest a linear relationship between these parameters. This is expectable, because graben width should be proportional to sand thickness as long as the angle of internal friction, ϕ, is about the same for all tests and initial graben faults meet at the sand/paraffin contact.

Finally, it was found that varying the thickness of the paraffin layer caused a corresponding variation in the number and spacing of grabens for a given sand thickness. No quantitative information was

obtained to illustrate this relationship. Generally, however, for models with 7 mm of paraffin the spacing of the grabens was about equal to the initial width of the grabens, whereas for models with 15 mm of paraffin the spacing was on the order of three times the initial width of grabens. This suggests that spacing of the model grabens may be controlled in part by thickness-dependent properties of the paraffin layer. It is possible that the spacing of grabens in Canyonlands may also depend on properties of the flowing evaporite layer, but I have no evidence to support or refute this possibility.

Validity of the Models

The demonstration models show that grabens will form when a layer of sand is extended on a layer of laterally spreading paraffin. Beyond this I have tried to show by analogy that the geometry of the experimentally produced grabens is in many ways similar to the geometry of Canyonlands grabens.

It is recognized that there are many problems involved in working with these or any other models. Specifically, it has been demonstrated that the origin of orthogonal joint sets in Canyonlands predated the faulting, and it was inferred that the joints may have formed in response to a different stress system. The fractures in the models, on the other hand, consisting of both extension and conjugate shear fractures, are due to a single deformation in which stresses are known to vary spatially and temporally. The model assumes isotropic and homogenous conditions for the prototype, an assumption that is seldom valid in nature and certainly not valid for rocks in Canyonlands. Finally, the curvature of the graben complex distinguishes the overall structure as nonprismatic.

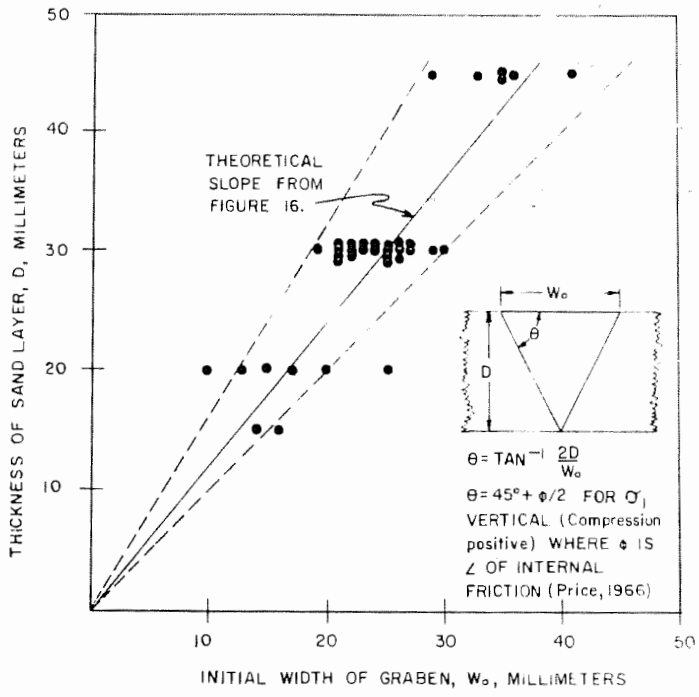

Figure 24: Plot of initial widths of scale model grabens vs. thickness of the sand layer. The solid line represents a fault dip of 67.5° (i.e., $\emptyset$ = 45°). The dashed lines enveloping all the data for models with a 30-mm-thick sand layer show a range in fault dips from 64° to 73°. This implies a range in internal friction from $\emptyset$ = 38° to $\emptyset$ = 56°.

- -

However, individual grabens approximate prismatic geometry whereas scale-model grabens obviously do not. These are but a few of the problems; more could be identified.

On the other hand, the model simulation indicates that Baker's hypothesis (1933) is mechanically sound and, in agreement with field observations, the best explanation for the origin of Canyonlands grabens. Because of numerous similarities in the surficial geometry of scale-

model grabens and Canyonlands grabens, the model simulation is useful to suggest constraints on the subsurface geometry of Canyonlands grabens. In a more general sense, the model simulation has provided an opportunity to study the growth of grabens and has supplied insights which have been helpful in understanding the origin of grabens in Canyonlands National Park.

KINEMATICS OF GRABEN GROWTH

Introduction

A kinematic model for the growth of grabens in the Lower Red Lake Canyon area has been developed from the synthesis of field observations and the results of simulation with geologic scale models. It is presented in the form of a short scenario describing inferred kinematics during four successive stages in the development of a single graben. A discussion following each stage of the scenario summarizes the important inferences and the evidence on which the kinematic interpretation is based. Examples of grabens in each of the four successive stages of growth are illustrated in Figure 26.

1. Incipient Graben

Kinematics. Initial failure of the brittle plate occurs in basal beds of the upper member of the Hermosa as shear fractures conjugate about σ_1 (compressive and approximatley vertical) and striking perpendicular to the extension direction. The mechanics of faulting, analyzed earlier in the paper, suggest that the fractures propagate toward the surface by following preexisting vertical joints in strong units and shearing on planes dipping about 65° in weak units. The average dip of the resulting through-going faults is about 85°.

The maximum width of the incipient graben is reached at marker d (Fig. 3) and averages between 80 and 100 m. Above this level, faults conform to open vertical master joints.

Discussion. The key inferences for this stage of graben growth are: (1) the faults bounding each graben begin at or very near the base

of the upper member of the Hermosa, and (2) the initial surface width is a function of the thickness of the brittle plate below open master joints. These inferences are supported by a number of geometric observations and interpretations.

The fact that the deformation has occurred as systematically spaced grabens of similar geometry, is good evidence that paired faults converge at depth. The alternate interpretation, that faults bounding the grabens are vertical through the thickness of the brittle plate (Baker, 1933; Lewis and Campbell, 1965), presents some serious problems. The asymmetry inherent in the subsurface flow mechanism would tend to produce independent normal faults favoring west-wall-down slip. If this is the case, it is not clear why the faults should be paired at all. Furthermore, McGill and Stromquist (1974, p. 18) have argued that a dynamic model assuming rigid graben blocks bounded by vertical faults is not acceptable, because evidence for differential uplift of intergraben divides, that should result due to volume displacement of evaporites, is generally absent.

Measurements of the width at the ends of simple grabens north of the Chesler Canyon lineament generally fall between 80 and 100 m. This observation suggests that paired faults intersect at a common depth. The obvious datum that is common to all grabens is the brittle/ductile contact. An average fault dip of 85°, below the depth of open master joints, allows the graben faults to intersect at the base of the brittle plate. This value was determined for an initial surface width of 80 to 100 m and is consistent with the average dips measured on the wall of Lower Red Lake Canyon.

Both the width and the depth to the floor of individual grabens increase along strike away from graben ends. It is interpreted from this observation and the consistent width at graben ends that the initial width at any point along strike is constant and also in the range of 80 to 100 m. This inference is supported by a plot of 25 width/depth measurements from selected cross sections of grabens in the north end of the fault complex (Fig. 25). The data were obtained from aerial survey contact prints by stereographic techniques. A linear regression through 19 data points (dark circles), representing cases where the faults show little modification by the processes of secondary

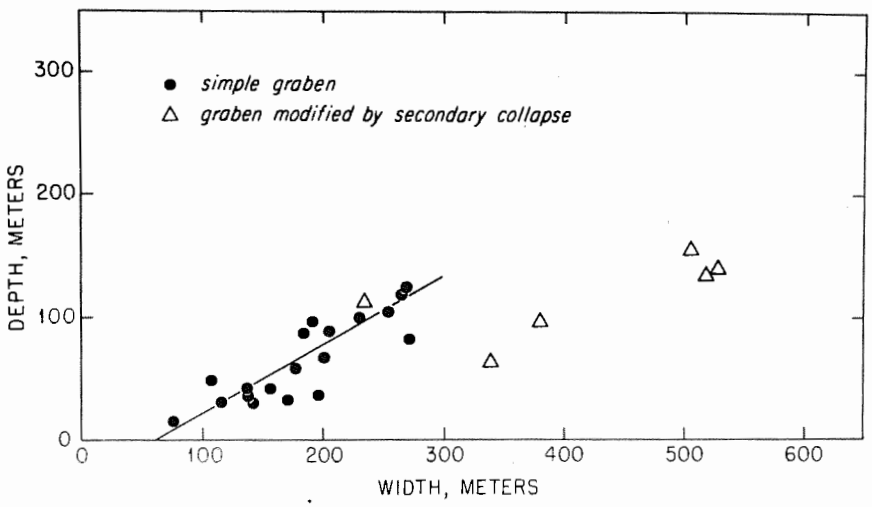

Figure 25: Plot of width and depth of grabens measured at selected localities north of the Chesler Canyon lineament. The data suggest a systematic relationship between width and depth for grabens up to about 300 m in width. Beyond this limit, processes of secondary widening unsystematically modify large grabens. A linear regression curve through 19 data points (dark circles) indicates an initial graben width (at 0 m displacement) of about 60 m. This value is in general agreement with field observations.

widening (Fig. 26b), suggests that the initial width of grabens is on the order of 60 m. To a first approximation, this value agrees with the range of observed end widths, because the accuracy of measurements from the stereograph is ±20 m at best.

It is inferred from the discussion of the sawtooth geometry of the fault scarps in an earlier section, that the strike of the faults at depth diverges from the trend of master joints in the near-surface rocks. This requires that the faults begin below the depth of open master joints and propagate toward the surface.

Drag folds mapped in the Rico and upper Hermosa demonstrate that some of the more elastic beds may sustain finite bending prior to failure as the faults propagate toward the surface.

2. Simple Graben

Kinematics. After the paired faults have propagated up to the surface, the downthrown block settles by equal and simultaneous displacements on both faults. Equal displacements create and maintain lateral symmetry. The adjacent downdip intergraben divide, which is now detached from the main body of rock except at the ends of the graben, continues to creep downslope as a gravity slide block. As the graben propagates along strike, the initial 80 to 100 m width is maintained at the ends. In areas where fault and joint trends diverge, grabens propagate along strike as a succession of en-echelon segments. Individual grabens die out in a series of ramping joint-block rows with average dips of about 10°. In earlier formed parts of the graben, the greater distance between fault scarps is the result of extension, which

of course, is accompanied by additional displacement of the downthrown block.

A consequence of the change in dip of the bounding fault from vertical near the surface, to steeply dipping at depth, is the formation of a gap between the downfaulted block and the fault scarps. The gap expands with increasing vertical displacement.

The slender point at the base of the downthrown block is easily crushed under the weight of the overlying rocks. Breccia is also formed along the 85°-dipping fault segments, as grinding between the upthrown and downthrown blocks smooths the step-like irregularities on the fault surface.

Discussion. The important elements in the early stage of graben growth are: (1) graben growth is characterized by lateral symmetry, and (2) the spacing between the fault scarps is a reliable measure of extension.

The symmetry of simple grabens is shown most clearly by the lack of tilting of the downthrown blocks. Lateral symmetry, geometry of graben ends, and the smooth continuity of the regional dip are additional evidence that the paired faults start contemporaneously at a common depth. Furthermore, these features provide sufficient evidence to reject the possibility that grabens form between a through-going master fault and an antithetic fault intersecting the master fault at some intermediate depth. It is not likely that a graben formed by this mechanism would demonstrate lateral symmetry, since displacement would first occur along the master fault, followed by growth of the antithetic

fault. In addition, initial displacement on the master fault would disrupt the continuity of the regional dip.

Direct evidence for the presence of gaps between the downthrown blocks and the fault scarps is provided by swallow holes along the scarps where internal drainage flows into the ground. In some cases it is possible to measure the width of the gap. The obvious lack of slickensides on the fault scarps is additional evidence that separation along the faults accompanied settling of the downthrown block. The loss of lateral confinement that occurs by enlargement of this space must give rise to instability that is further intensified by the presence of additional master joints adjacent and parallel to the faults. Thus, the initial fault scarps are essentially free-standing joint-bounded slabs. In young grabens where the vertical displacements are small, the space may only be a few meters wide, so that accumulation of windblown sand and silt, alluvium, and rubble would act to buttress the scarps, thereby reducing the instability.

3. Intermediate Graben

Kinematics. In the intermediate stage, propagation along strike declines, but extension continues by slow gravity sliding of the detached intergraben divide. The rate at which the detached block moves is greatest near the widest part of the adjacent graben, but obviously decreases to near zero at the ends of the graben where it remains pinned to the main body of the brittle plate.

As the vertical displacement of the downthrown block approaches the depth to which master joints are open ($\sim$100 m) the potential void along the sides of the block may be tens of meters across, so that joint-

bounded slabs of near-surface rock would be free to rotate away from the walls and collapse into the graben. Commonly, these slabs will shear at depth after only a small amount of rotation. Rubble from the collapsed slabs will either contribute to filling the voids or will accumulate as talus.

The downthrown block does not penetrate into the Paradox Member. Instead, the block fails by internal shearing and is thus able to fill available space. Breccia formed near the base and along the sides of the block is also redistributed to fill voids created by fault separation.

Discussion. The key inferences for the intermediate stage of graben growth are: (1) displacement of the downthrown block continues during extension so that the depth of the block is a function of the age of the graben, (2) vertical fault segments are modified by wall collapse producing secondary widening, and (3) the downthrown block does not penetrate into the flowing layer.

Many examples of joint-bounded slabs, at various stages of rotation away from the graben walls, were observed in the Lower Red Lake Canyon area. McGill and Stromquist (1974, Fig. 16) used a series of cartoons to illustrate how inward rotation and collapse might operate to partially fill the space along the sides of the downthrown block. Because the instability increases as the gap expands, the process of wall collapse is more likely to operate as displacement of the downthrown block becomes very large. The cumulative effect of activity along the fault scarps is to produce secondary widening near the surface. Thus, when a graben has reached intermediate stage, the width of the graben is no longer a measure of the distance between the fault scarps, and therefore,

it is no longer a reliable measure of extension. Also, debris from collapsed slabs accumulates with alluvial and eolian deposits on the floor. Consequently, the depth to the graben floor may not be a valid estimate of the depth to the top of the downthrown block.

The limited penetration of the downfaulted block into the Paradox Member was suggested by the geologic scale models. It was observed that sand grains at the base of the scale-model grabens do not penetrate into the paraffin layer. Although the paraffin deformed plastically, to individual sand grains the paraffin behaved as highly viscous material. Thus, basal sand grains supported overlying sand and the downfaulted material was redistributed under its own weight to fill the available space. By analogy, it is suggested that although the Paradox Member contains very mobile strata, demonstrated by exposures of sheared evaporites along Cataract Canyon, it also behaved as a highly viscous material to individual breccia blocks at the base of the grabens. No direct evidence was found because there are no exposures of graben faults at the upper contact of the Paradox Member, but evidence of internal failure was observed in Twin and Unnamed Canyons in the form of differentially faulted joint-bounded blocks of Cedar Mesa Sandstone on the graben floors. Certainly, some tectonic mixing of breccia with the Paradox Member is inevitable, but because of volume displacement constraints discussed earlier, the fraction of the original volume of the graben block lost to tectonic mixing is considered to be small.

4. Large, Complex Graben

Kinematics. Internal shearing and brecciation of the downthrown block continue. Extreme secondary widening occurs when massive slabs

hundreds of meters long and 30 to 40 m wide are downfaulted and rotated away from the graben walls. Small grabens commonly form behind these rotated slabs. Thick talus prisms accumulate along the bases of scarps as a result of simple wall collapse.

Arching due to the rise of evaporites beneath large grabens is expressed at the surface as outward rotation and warping of adjacent intergraben divides. Secondary grabens form on the interior regions of these divides. Those with sawtooth fault scarps are initiated at depth, while others with faults that follow a single master joint might form near the surface.

Discussion. Exposures of downthrown blocks are rare, due to thick eolian and alluvial deposits on the graben floors. Also, because the original faults are buried by inward-rotated slabs and extensive talus, even their approximate locations are doubtful. Thus, the geometry of the downthrown blocks must be inferred from observations of less complex grabens.

One of the problems of large grabens is the geometry of inward-rotated slabs. If a large graben evolved from a simple graben as assumed, then the structure of the inward rotated slabs is not compatible with the kinematics of secondary widening in the intermediate stage. However, because the subsurface geometry of a large complex graben is not known, it is also not known if the same kinematics operate in the advanced stage of growth.

Relative Age Criteria and Sequence of Graben Growth

According to the preceding kinematic interpretation, graben depth is a function of age, because displacement of the downthrown block continues with extension. It has been demonstrated that the relationship between width and depth is systematic in early stages of growth (Fig. 25). In later stages, wall collapse unsystematically modifies fault scarps, with the result that surface width increases more rapidly than depth. Because processes of wall collapse are more likely to operate as depth becomes large, it follows that the extent of secondary widening is also a function of the age of a graben. Therefore, width,

- -

Figure 26: Examples of grabens in four successive stages of growth taken from the vicinity of Lower Red Lake Canyon.

a. Incipient graben (upper left). View looking north along Devil's Lane graben. The left en-echelon continuation is the Twin Valleys graben. The distance between faults is about 100 m. The end of a simple graben must be used to illustrate the surface geometry of a graben with no displacement.

b. Simple graben (upper right). View south along Devil's Lane graben. The Twin Valleys graben referred to in the previous photograph is in the right foreground.

c. Intermediate graben (lower left). Cyclone Canyon graben seen looking south. The width varies from 100 to 250 m and the depth from 50 to 100 m.

d. Large, complex graben (lower right). View of Red Lake Canyon graben, looking south. The width is on the order of 500 m and the depth about 140 m.

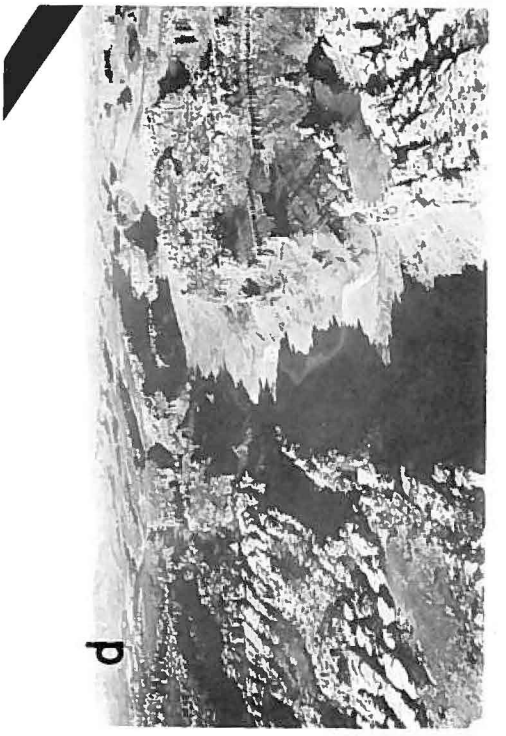

depth, and the effects of secondary widening can be used as relative age indicators.

When the age criteria are applied to grabens north of the Chesler Canyon lineament (Fig. 4), it is seen that Red Lake Canyon, an anomalously wide, deep graben showing extensive modification along the scarps, is the oldest graben. In this scheme, the overall geometry of grabens east of Red Lake Canyon suggests that these grabens are progressively younger up the regional dip toward Devil's Pocket. The latter, a narrow, shallow graben showing little or no modification along the fault scarps, is the youngest in this series. Furthermore, each of the grabens becomes younger along strike to the northeast. It is interesting to note that the same age sequence characterized the growth of experimental grabens.

The overall geometries of Lens, Twin, and Unnamed Canyons suggest that these grabens are in an intermediate to advanced stage of growth. There are sufficient similarities between these structures and the Cyclone Canyon graben to make age correlation tempting; however, contemporaneous growth of the four structures is contrary to the updip age sequence that has been proposed. Alternately, the three grabens may have formed very late, following decline in the rate of extension to the east, or a different mechanism may have operated to form grabens west of Red Lake Canyon. In any case, the relative age of grabens west and east of Red Lake Canyon is not clearly established.

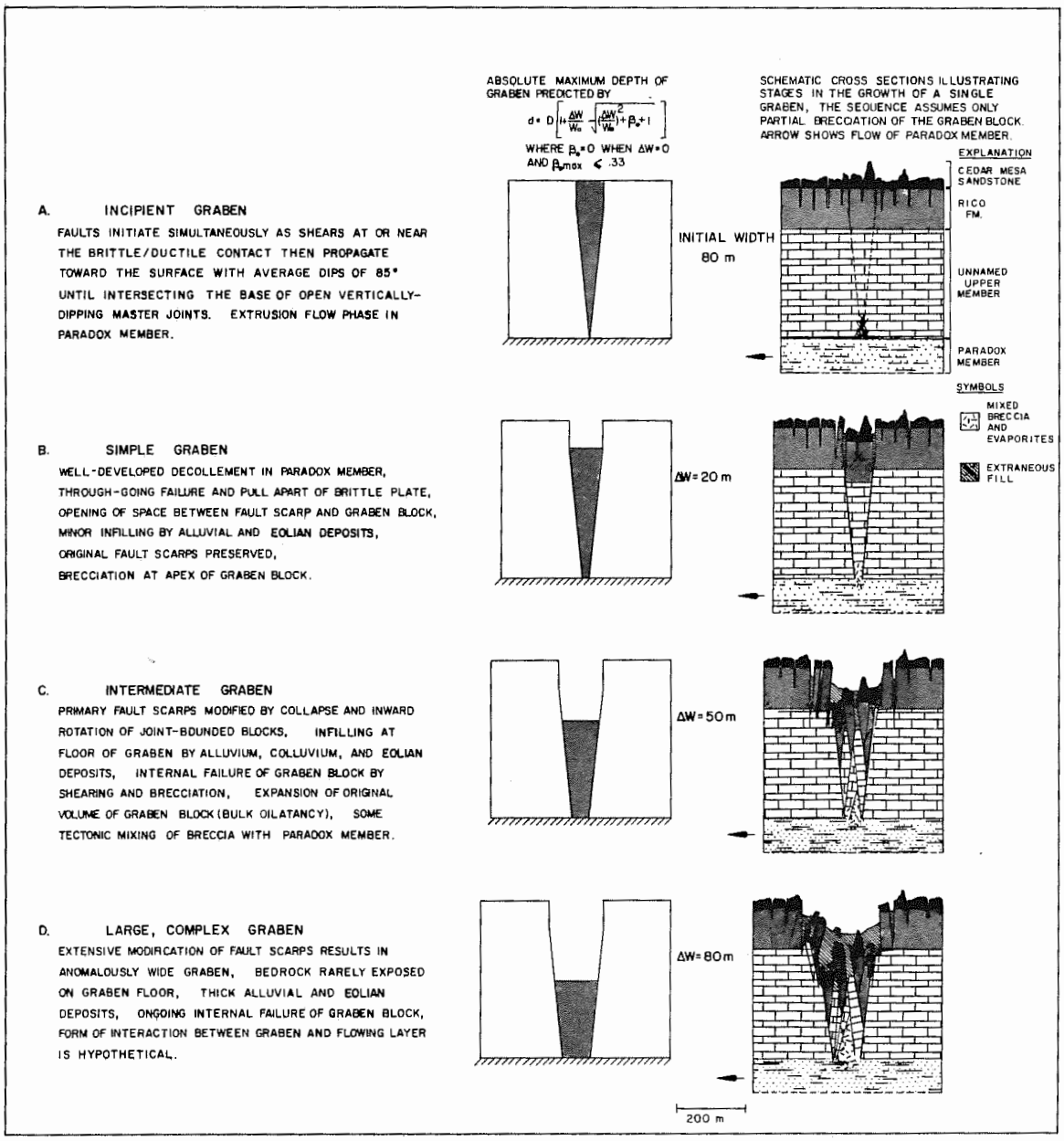

Figure 27: Summary of the kinematic model for graben growth illustrating sequential development of a single graben. The interpretation of subsurface geometry illustrated in the right hand column is consistent with the structure of the near-surface rocks.

Volumetric Method for Predicting Depth to the Flowing Layer

Derivation. Geometric and mechanical constraints imposed on graben formation by the kinematic model (Table 1) are useful to derive a method for predicting depth to the flowing layer. The derivation is based on a simple geometric model that assumes: (1) intersection of uniformly dipping paired faults at the base of the brittle plate, (2) extension of the brittle plate by simple lateral translation, (3) no penetration of the downthrown block into the flowing layer, (4) internal shearing and brecciation of the downthrown block to fill available space; and (5) no addition of extraneous material.

To account for the overall average fractional increase in volume of the original graben block, the term bulk dilatancy, β_o, is introduced. It is emphasized that this term is not a measure of the aggregate volume increase through expansion of single grains. Rather, β_o expresses the cumulative effect of the megascopic voids formed as a result of internal failure.

It is a simple matter to write expressions for the total space to be filled after finite extension, the amount of total space occupied by the original volume of the graben block allowing for increase in volume through bulk dilatancy, and the amount of total space remaining above the graben floor. The result of combining and simplifying these expressions is a nonspecific quadratic equation that relates initial and final width, thickness of the brittle plate, depth to the top of the downthrown block, and the bulk dilatancy (Fig. 28, expression 4). The solution to this volumetric problem was first obtained by McGill

Table 1: Summary of interpretations and constraints on the kinematic model.

Observations and Assumptions	Interpretations and Constraints
1. Brittle layer overlying mobile layer.	1. Brittle layer overlying mobile layer.
2. Brittle layer fails on steeply dipping but not vertical faults.	2. Steep fault dips controlled by bedding and fracture anisotropies.
3. Sawtooth pattern of fault scarps.	3. Faults initiate in the subsurface and propagate up through the brittle layer.
4. Continuity of prefaulting erosional surface; relative uplift or subsidence of intergraben divides not common.	4. Extension by simple lateral translation.
5. Symmetry of grabens demonstrated by lack of lateral tilting of downthrown block.	5. Grabens not formed by master faults and antithetic faults. Instead grabens form between contemporaneous normal faults.
6. Deformation has produced systematically spaced grabens with similar geometries.	6. Paired faults converge and intersect at base of brittle plate.
7a. Grabens die out along parallel faults.	7a. Principal bounding faults initially parallel.
b. Depth increases systematically with width in individual simple grabens.	b. Distance between faults is a measure of extension.
c. Average width of 80 to 100 m at the ends of grabens.	c. Grabens form with constant initial surface width of 80 to 100 m.
8. Assumed rheology of brittle rocks and evaporites.	8a. Downthrown block does not penetrate into flowing layer.
	b. Graben block fails by internal shearing and brecciation.

(pers. commun., 1975) through a more cumbersome derivation than the one shown in Figure 28.

The derivation is simplified by disregarding the near-surface vertical portion of the principal bounding faults. This is a valid approximation, if the depth of the vertical portion is small compared to

the thickness of the brittle plate, and the hade of the dipping fault segment does not increase with depth. The derivation for the specific case, where the effect of the vertical scarps is considered, necessarily contains additional terms which do not contribute to a basic understanding of the method.

Application. Three useful relationships follow from this quadratic equation for cases in which the values of all but one of the variables are theoretically known. In the case of the geologic scale models, both the initial and final dimensions are known, so that by applying expression 5 (Fig. 28), characteristic values of β_o for the sand/powder mixture can be calculated. Table 2 summarizes the results of calculations for individual grabens from four experiments. Because the β_o term in the models is physically a measure of the "unpacking" of sand grains through internal failure of the graben "blocks", it seems unlikely that the values of β_o should exceed 1/4 to 1/3 of the original volume. Of course, for the relationship to be applicable, each graben must conform to the geometry shown in Figure 28. Where paraffin ridges have formed beneath grabens and when the growth of paraffin ridges has been sufficient to cause outward rotation of the graben faults the relationship ceases to be valid. Some large values of β_o, greater than .3 and up to 1.5 for example, may represent cases where either or both of these conditions exist.[1] Open fractures near the top of the downfaulted sand, due to

[1] Some Canyonlands grabens may be underlain by evaporite ridges, but there is no direct evidence to prove the existence of such features. Similarly, it is difficult to distinguish the presence of paraffin ridges beneath model grabens by the same set of observations used in the prototype area. Hence, data for these scale-model cases are included in Table 2 to make the analogy between model and prototype more general.

FIGURE 27. DERIVATION OF AN EXPRESSION FOR PREDICTING DEPTH TO THE FLOWING LAYER.

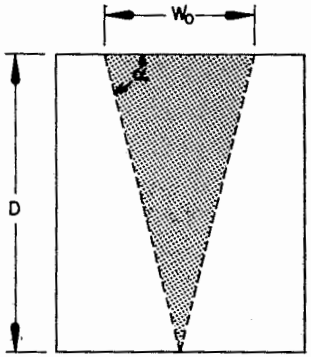

INITIAL GEOMETRY

VOLUME OF INCIPIENT GRABEN PER UNIT LENGTH NORMAL TO PLANE OF DRAWING = $1/2 \cdot W_o \cdot D$

$$\text{TAN } \alpha = \frac{D}{1/2\ W_o}$$

EXPLANATION OF VARIABLES:

- W_o = INITIAL WIDTH OF GRABEN
- D = DEPTH TO FLOWING LAYER
- d = DEPTH TO GRABEN FLOOR
- ΔW = CHANGE IN WIDTH
- α = ANGLE OF DIP ON FAULTS
- β_o = BULK DILATANCY (FRACTIONAL INCREASE IN THE ORIGINAL VOLUME OF THE DOWNTHROWN BLOCK.)

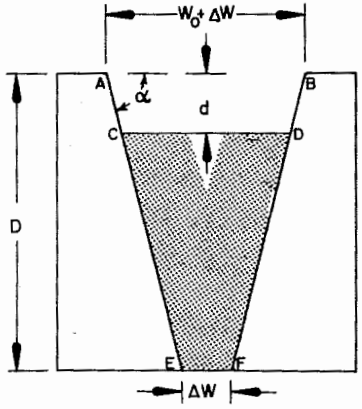

AFTER FINITE EXTENSION

BASED ON THE FOLLOWING ASSUMPTIONS:

1. THE DOWNTHROWN BLOCK DOES NOT PENETRATE INTO THE FLOWING LAYER
2. THE DOWNTHROWN BLOCK FAILS BY INTERNAL SHEARING AND COMPLETE BRECCIATION TO FILL THE AVAILABLE VOLUME
3. NO EXTRANEOUS MATERIAL IS ADDED.

TOTAL SPACE TO BE FILLED = $1/2 \cdot W_o \cdot D + \Delta W \cdot D$

AMOUNT OF TOTAL SPACE OCCUPIED BY AVAILABLE MATERIAL = C-D-E-F = $(1+\beta_o) \cdot 1/2 \cdot W_o \cdot D$

AMOUNT OF TOTAL SPACE ABOVE GRABEN FLOOR = A-B-C-D = $d \cdot (W_o + \Delta W - d / \text{TAN } \alpha)$

THUS: $1/2 \cdot W_o \cdot D + D \cdot \Delta W = (1+\beta_o) \cdot (1/2 \cdot W_o \cdot D) + d \cdot (W_o + \Delta W - d / \text{TAN } \alpha)$

SUBSTITUTING THE EXPRESSION FOR TAN α INTO THE EQUATION ABOVE:

$$1/2 \cdot W_o \cdot D + D \cdot \Delta W = (1+\beta_o) 1/2 \cdot W_o \cdot D + d(W_o + \Delta W) - \frac{d^2 W}{2D_o} \qquad (1)$$

MULTIPLYING BOTH SIDES OF THE EXPRESSION TO CLEAR FRACTIONAL TERMS:

$$D^2 W_o + 2D^2 \Delta W = (1+\beta_o) D^2 W_o + 2Dd(W_o + \Delta W) - d^2 W_o \qquad (2)$$

COMBINING LIKE TERMS AND SIMPLIFYING:

$$D^2 (2\Delta W - \beta_o W_o) - 2Dd(W_o + \Delta W) + d^2 W_o = 0 \qquad (3)$$

FACTORING A W_o FROM EACH POLYNOMIAL TERM IN EQN. 3 AND SIMPLIFYING:

$$D^2 (2 \frac{\Delta W}{W_o} - \beta_o) - 2Dd(1 + \frac{\Delta W}{W_o}) + d^2 = 0 \qquad (4)$$

SOLUTION FOR β_o FROM EQN. (4) YIELDS AN EXPRESSION FOR BULK DILATANCY IF THE DIMENSIONS OF THE GRABEN ARE COMPLETELY KNOWN.

$$\beta_o = (\frac{d}{D})^2 - 2\frac{d}{D}(1 + \frac{\Delta W}{W_o}) + 2\frac{\Delta W}{W_o} \qquad (5)$$

SOLUTION FOR d FROM EQN. (4) YIELDS AN EXPRESSION FOR DEPTH OF THE GRABEN FOR SELECTED VALUES OF β_o WHEN D, W_o, AND ΔW ARE KNOWN.

$$d = D\left\{1 + \frac{\Delta W}{W_o} - \left[(\frac{\Delta W}{W_o})^2 + \beta_o + 1\right]^{1/2}\right\} \qquad (6)$$

THE NEGATIVE VALUE OF THE SQUARE ROOT IS REQUIRED SINCE THE EXPRESSION INSIDE THE BRACKETS MUST BE LESS THAN 1 IF D>d AS ASSUMED.

SOLUTION FOR D FROM EQN. (4) YIELDS AN EXPRESSION FOR DEPTH TO THE FLOWING LAYER FOR SELECTED VALUES OF β_o WHEN d, W_o, AND ΔW ARE KNOWN.

$$D = d\left\{\frac{1 + \frac{\Delta W}{W_o} + \left[(\frac{\Delta W}{W_o})^2 + \beta_o + 1\right]^{1/2}}{2\frac{\Delta W}{W_o} - \beta_o}\right\} \qquad (7)$$

THE POSITIVE VALUE OF THE SQUARE ROOT IS REQUIRED SINCE THE EXPRESSION INSIDE THE BRACKETS MUST BE GREATER THAN 1 IF D>d AS ASSUMED.

strength of the limestone, also increase the magnitude of β_o. Finally, errors as small as 10 percent in measurements of the final width and depth can cause β_o to vary by factors of up to 3. The results of the analysis of model grabens to determine β_o values is somewhat equivocal. Although no specific values for bulk dilation of dry sand have been found from the literature, it is suggested that values up to .3 are reasonable. Beyond this limit, it is expected that measurement errors or departures from ideal geometry of the type discussed above have contributed significantly to large values of β_o (Fig. 29).

In the case of Canyonlands grabens, it is necessary to consider the effect of adding extraneous material to the total volume to be filled. For this purpose β can be thought of as the sum of two components, one expressing volume increase of the graben block through internal failure, β_o, and the other representing the contribution of extraneous fill to the total volume of material filling the available space. The latter can be represented by a dummy parameter, subsequently referred to as β_e, which expresses the volume of extraneous material as a function of the initial volume of rock in the graben. Extraneous fill includes alluvial and eolian fill in addition to debris derived from collapse along the fault scarps.

When expression 5 (Fig. 28) is used to determine characteristic values of β for Canyonlands grabens, results are obtained that are very different from values of β_o determined for model grabens. To use this equation, it must be assumed that the end width of a graben is a measure of the initial width at any point along the graben. Then by measuring

Table 2. Results of applying expression 5 to scale-model grabens from selected experiments with 30 mm sand layer.

W_o mm	Final Width mm	$\frac{\Delta W}{W_o}$	Thickness D mm	Depth d mm	$\frac{d}{D}$	β_o
17.0	25.0	0.47	30.0	2.0	0.06	0.74
22.0	32.0	0.45	30.0	2.0	0.06	0.71
18.0	25.0	0.38	30.0	3.0	0.10	0.51
20.0	28.0	0.40	30.0	3.0	0.10	0.53
24.0	31.0	0.29	30.0	4.0	0.13	0.25
25.0	34.0	0.36	30.0	7.0	0.23	0.13
23.0	42.0	0.82	30.0	15.0	0.50	0.07
22.0	34.0	0.54	30.0	4.0	0.13	0.69
23.0	28.0	0.21	30.0	2.0	0.06	0.27
24.0	46.0	0.91	30.0	10.0	0.33	0.66
18.0	32.0	0.77	30.0	4.0	0.13	1.09
24.0	35.0	0.45	30.0	7.0	0.23	0.29
22.0	57.0	1.59	30.0	11.0	0.36	1.41
25.0	30.0	0.20	30.0	4.0	0.13	0.09
13.0	18.0	0.38	30.0	3.0	0.10	0.50
14.0	16.0	0.14	30.0	1.5	0.05	0.17
12.0	15.0	0.25	30.0	3.0	0.10	0.26
12.0	18.0	0.50	30.0	5.0	0.16	0.52
16.0	31.0	0.93	30.0	7.0	0.23	1.02
16.0	20.0	0.25	30.0	3.0	0.10	0.26
14.0	18.0	0.28	30.0	2.0	0.06	0.40

- -

the final width and depth to the graben floor and using the thickness of the brittle plate (460 m) as the depth to the flowing layer, values of β can be computed.

The results of applying expression 5 (Fig. 28) to the width and depth measurements plotted on Figure 25 are summarized in Table 3. Here the computed value of β includes both the bulk dilatancy, β_o, and the volume fraction of extraneous fill, β_e. There are several feasible uncertainties or sources of error that can account, at least in part,

for the unreasonably large values of β in Table 3. They are as follows:

1. Width and depth measurements obtained from air photographs may be inaccurate if parallax was not fully compensated by calibration of the Zeiss Stereotope.

2. The effect of 90° near-surface fault dips was neglected for computing bulk dilatancy.

3. The magnitude of β_o is clearly an unknown, although geometric arguments may provide reasonable estimates.

4. Tectonic mixing between evaporites and the graben blocks may not be negligible.

5. The value of depth to the flowing layer (460 m) depends on the accuracy of the stratigraphic section measured in Lower Red Lake Canyon and may be subject to areal variation.

6. The thickness of extraneous material on graben floors is generally not known and therefore, graben depth may not be an accurate measure of vertical displacement.

7. The final width cannot be determined accurately in grabens that have undergone extensive secondary widening by wall collapse.

8. The end width of grabens may not be a valid approximation of the initial width if the dip of the faults varies systematically along strike.

The first five possible sources of error or uncertainty in the preceding list, acting either separately or in combination, could not

Table 3. Results of applying expression 5 to width and depth measurements from Canyonlands as plotted on Figure 25.

W_o meters	Final Width meters	$\frac{\Delta W}{W_o}$	Thickness D meters	Depth d meters	$\frac{d}{D}$	β_o
80.0	115.8	0.44	460.0	30.4	0.06	0.70
80.0	137.1	0.71	460.0	36.5	0.07	1.16
80.0	195.0	1.43	460.0	36.5	0.07	2.49
80.0	143.2	0.79	460.0	30.4	0.06	1.34
80.0	170.6	1.13	460.0	33.5	0.07	1.95
80.0	201.1	1.51	460.0	67.0	0.14	2.31
80.0	137.1	0.71	460.0	42.6	0.09	1.11
80.0	192.0	1.40	460.0	91.4	0.19	1.88
80.0	381.0	3.76	460.0	97.5	0.21	5.55
80.0	338.0	3.22	460.0	64.0	0.13	5.29
80.0	265.2	2.31	460.0	189.0	0.41	2.07
80.0	518.0	5.47	460.0	134.0	0.29	7.26
80.0	527.0	5.58	460.0	140.0	0.30	7.25
80.0	204.0	1.55	460.0	88.0	0.19	2.16
80.0	253.0	2.16	460.0	104.0	0.22	2.94
80.0	235.0	1.93	460.0	113.0	0.24	2.49
80.0	182.0	1.27	460.0	88.0	0.19	1.71
80.0	106.0	0.32	460.0	49.0	0.10	0.37
80.0	177.0	1.21	460.0	58.0	0.12	1.88
80.0	156.0	0.95	460.0	42.0	0.09	1.55
80.0	271.0	2.38	460.0	81.0	0.17	3.61
80.0	506.0	5.32	460.0	155.5	0.33	6.48
80.0	269.0	2.36	460.0	125.0	0.27	2.97
80.0	230.0	1.87	460.0	99.0	0.21	2.55

account for more than a small part of the large values of β. The three remaining factors are important and require some additional explanation.

The effects of secondary widening are generally minor or even absent in simple grabens. Reasonable results are expectable if the volumetric model is applied to these simple grabens because accurate

measurements of final width, initial width, and vertical displacement are possible. This assumes that extraneous deposits on the graben floors are negligible, original fault scarps form the existing graben walls, and the end widths are a valid approximation of the initial widths in the deeper parts of the grabens. In intermediate to large complex grabens, on the other hand, the effects of secondary widening are extensive. The principal result is that joint faces forming the original fault scarps are destroyed by collapse of the first joint block row. Collapse of successive joint-bounded blocks adds to the apparent width of the grabens. If the model is applied to these grabens, the final width will be overstated if measured as the distance between existing graben walls. Furthermore, collapsed joint block rows accumulate on the top of the downthrown block with alluvium and eolian deposits. Hence, the amount of vertical displacement will be understated if measured as the depth of the graben beneath the surface of the adjacent upthrown blocks.

The problems introduced by secondary widening are compounded if the initial width is not constant, but is affected by longitudinal variation in fault dips. It is possible that variation in total stress, due to increase in strain rate towards the widest parts of the grabens, could cause significant changes in fault dips. Variation in the mechanical properties of the brittle layer could also affect fault dips, but no significant changes in lithology were observed along the strike of the faults that might account for such variation.

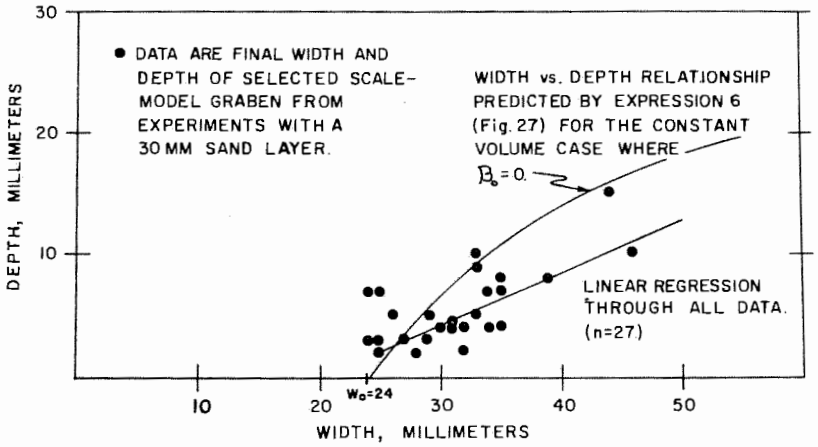

Figure 29: Plot comparing width and depth of selected scale-model grabens to ideal values predicted by the volumetric model. The ordinate difference between the two curves should reflect the bulk dilation, but because the data are scattered, the probability is high that the slope of the regression is steeper and hence, the apparent β_o is smaller. Also, because the initial widths of grabens vary by several millimeters, better agreement would be expected between measured and predicted depth to width relationships for individual grabens.

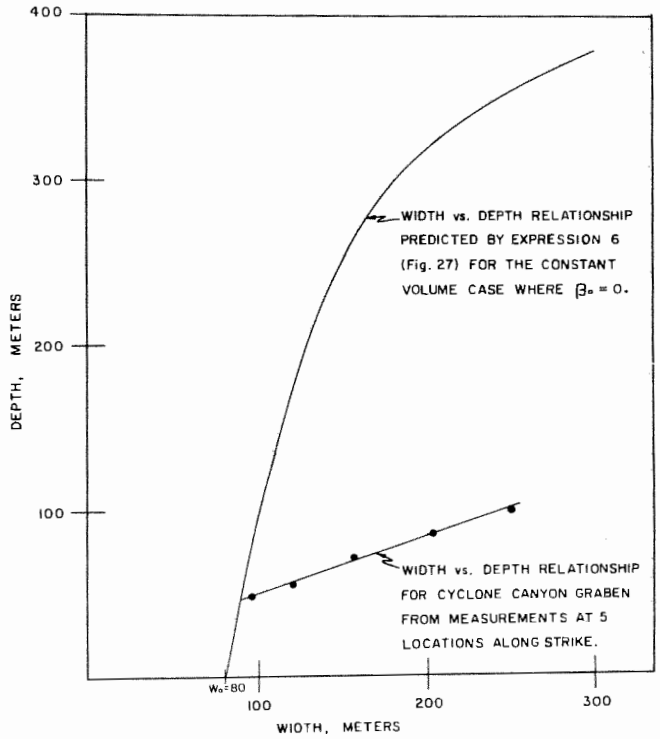

Figure 30: Plot comparing width and depth measurements along Cyclone Canyon to ideal values predicted by the volumetric model.

It is suggested from the preceding discussion that overstating final width and understating initial width and vertical displacement in intermediate to large complex grabens could account for the results in Table 3, because all affect computations of β in the same direction. The same combination of errors could also account for the lack of agreement between width and depth measurements along the Cyclone Canyon graben and ideal values predicted by the volumetric model (Fig. 30).

Despite the several sources of error, the model remains a viable one. It has the benefit of being internally consistent with the geometry of Canyonlands grabens and the mechanical properties of the rocks. Through equation 7, the model provides a means for estimating depth to the flowing layer, that is applicable to grabens where initial width, final width, and depth of the downthrown block are known. Also, because of the many sources of error involved in estimating the cross-sectional dimensions of a graben, the bulk dilatancy term, β_o, may be neglected in most cases without seriously affecting computations of depth to the flowing layer.

SUMMARY AND DISCUSSION

There can be little remaining doubt that formation of the Canyonlands grabens is a direct consequence of the mobility of the Paradox strata. McGill and Stromquist (1974) demonstrated the validity of Baker's (1933) hypothesis with limited field data and the results of early laboratory experiments with geologic scale models. The present study, although reaffirming the validity of a previously accepted hypothesis, has shown that although Baker recognized subsurface flow as the governing factor in the origin of the grabens, his model, nevertheless, contains several inaccuracies and misconceptions.

It is clear from Baker's discussion that he envisioned extrusion of evaporites from beneath the faulted zone into the Meander anticline like toothpaste from a tube, followed by uneven in situ settling of blocks of various size between vertical, parallel faults (1933, p. 74 and Plate 1). One would expect that the massive limestone and sandstone sedimentary cover should have sustained significant extension during extrusion of evaporites, particularly after the continuity of the cover was broken by the formation of grabens. Thus, it is difficult to imagine how wholesale extrusion flow of evaporites could have occurred while the overlying brittle plate remained essentially in situ. Furthermore, Baker has shown a progressive increase in the width of blocks westward toward Red Lake Canyon, suggesting that he used the distance between the graben walls as a reliable measure of the width of the downthrown block. This interpretation of the subsurface geometry neither explains how the width

would increase systematically downdip nor does it account for the consistent width of 80 to 100 m at the ends of grabens. Finally, Baker implies that the Paradox Member must have been like a sea of evaporites on which the overlying cover foundered and broke up during extrusion flow (Baker, 1933, p. 74). However, this theory does not account for the smooth continuity of the regional dip demonstrated by projecting bedding contacts across grabens, and it does not account for the uniform spacing of grabens. In the present investigation, a new model for graben growth has been developed that offers solutions to these problems. The concepts and conclusions from which the model was derived are summarized below.

It is generally agreed that the faulting was a response to tensile stresses superposed on the brittle rocks overlying the evaporites and acting parallel to the regional dip (Lohman, 1974). A shear couple superposed on the base of the brittle plate by viscous drag of flowing evaporites, when resolved into its principal stress components, could provide a tensile stress sufficient to increase the stress difference $(\sigma_1 - \sigma_3)$ to the point where faulting is initiated. Once the continuity of the brittle plate has been broken, extension continues as gravity sliding of the detached segment of sedimentary cover. Subsequent grabens would develop sequentially updip, as evaporites first actively tore apart the overlying cover during the extrusion flow phase and then provided lubrication for passive downslope sliding of detached inter-graben divides. A limit to the amount of extension that can occur by

gravity sliding is imposed by the observation that intergraben divides are not detached from the unfaulted part of the brittle plate at the ends of the grabens.

Faults are vertical within 100 m of the surface, where they follow preexisting master joints in the uneroded Cedar Mesa Sandstone and uppermost Rico Formation, but are clearly not vertical at depth, although dips measured in Lower Red Lake Canyon commonly exceed 80°. Step-like blocks along Cataract Canyon downthrown on single faults demonstrate toreva-type rotation. This is additional evidence that the brittle plate does not fail along vertically dipping faults below 100 m.

It is inferred from the observed geometry of grabens and the interaction of joints and faults that faulting initiated at or near the brittle/ductile contact and that paired faults propagated from this zone toward the surface by slip along old fractures and shearing across weak rocks. The resulting average dip of the through-going faults is about 85°. Near-surface displacement followed preexisting master joints in the Cedar Mesa Sandstone. The initial spacing between the faults at the surface is thus a function of the thickness of the brittle plate below the depth of open master joints and the mechanical properties of the rocks.

A consequence of vertical faults at the surface is that the scarps become unstable as a gap opens along the sides of the downthrown block. This leads to inward rotation and collapse of near-surface rocks in the

form of joint-bounded slabs. Baker, however, inferred that these slab-like blocks are bounded by through-going vertical faults parallel to the limiting faults (1933, p. 74). McGill and Stromquist (1974, Fig. 16) showed how rotation of joint-bounded slabs into the graben provides a mechanism for secondary widening. Hence, the distance between graben walls is not always a valid approximation of the distance between fault scarps. The fact that the grabens become wider from Devil's Pocket toward Red Lake Canyon is in part a function of extension, but also reflects increased activity along the fault scarps in the form of inward rotation and collapse with increasing vertical displacement.

It is assumed that only a small fraction of the original volume of each graben block is lost to tectonic mixing with the flowing Paradox evaporites.

I have developed a model for the origin and growth of grabens and have carried this model through to its logical end. After exploring all of its ramifications I find that the model is apparently not valid for large grabens, particularly those mapped in the Lower Red Lake Canyon area. The first significant anomaly was recognized when the expression for bulk dilatancy, $\beta = \beta_o + \beta'_e$, was evaluated for measured values of width and depth in Canyonlands grabens. When applied to Canyonlands grabens, β is only a convenient means of resolving the measured depth of the grabens with the total space that must be filled according to the model. As such, it is completely independent of how the downthrown block fails or whether, in fact, it fails at all. One way to account for values of β up to 700 percent was by an enormous thickness of

extraneous material on the floors of the grabens. In view of the youthfulness of the grabens and the low rate of erosion in the area this seems unlikely. Furthermore, recent field studies suggest that the thickness of alluvial and eolian deposits on the floors of the grabens is on the order of 5 to 10 m (G. E. McGill and D. B. Potter, pers. commun., 1975), so that most of the assumed large volume of extraneous fill must come from graben walls as talus and collapsed blocks.

Unreasonably large values of β are obtained if final width is overstated, and depth and initial width are understated, since all work in the same direction and could all logically happen in the same place. Because large β values were calculated even for simple grabens where secondary widening is presumably not a problem and final width and depth can be measured confidently, it is concluded that initial width is the key factor in a model for graben growth. Severe geometric problems encountered while trying to illustrate graben growth in cross section, assuming initial width to be both known and constant, support the validity of this conclusion. For example, the amount of internal shearing and jostling of blocks, that was required to illustrate a two-fold increase in width (Fig. 27D), is not adequately justified by field observation. I found it necessary to account for a very large portion of the grabens as alluvial and eolian deposits intermixed with rubble from collapsed slabs or as tectonically mixed breccia and evaporites at the base of the block. Up to a point, collapse of joint-bounded slabs accounts for some of the width of grabens, but beyond this point the mechanics of secondary widening become increasingly more difficult to

illustrate. These problems would be compounded in a cross section showing a four-fold increase in width as suggested by Red Lake Canyon. Alternatively, the kinematic model may never have applied to Red Lake Canyon or to similar large, complex grabens.

One of the important ramifications is that the extension determined for each graben must be accounted for by erosion along Cataract Canyon. Thus, if each of the large grabens has sustained a two-fold or greater increase in width, as the model suggests, one might ask if erosion and removal of the leading edge of the extending block by the Colorado River could have kept pace with the supply of new material.

Basically, I am concerned with a number of obvious discrepancies between the observed geometry of large grabens and the geometry at depth predicted by the model. Hence, for the foregoing reasons, I presently favor an alternative model for the large grabens in which larger initial widths occur as a result of lower average fault dips. I have no evidence to say whether this variation is governed by rate of flow, lithologic changes, or other factors. Although the alternative model cannot provide a method for estimating depth to the flowing layer, it can eliminate otherwise serious geometric problems.

CONCLUSIONS

1. Cataract Canyon and its major tributary drainages, particularly Lower Red Lake Canyon, were deeply entrenched when faulting occurred.

2. The mechanical boundaries on the flowing Paradox strata consist of a free face of sorts along Cataract Canyon, a stratigraphic pinchout of the evaporites south of Gypsum Canyon, a change in regional dip near the confluence of the Green and Colorado Rivers from westward to northward, and an updip limit to subsurface flow to the east and southeast.

3. Normal faulting associated with the development of grabens postdates the origin of the two sets of nearly orthogonal vertical joints. Furthermore, the overall trends of the faults are independent of the orientations of the joints.

4. Within 100 m of the surface the shear strength of the rocks is not exceeded, and faulting takes the form of separation along vertical master joints. Below this depth, paired faults with average dips of 85° converge and meet at or very near the brittle/ductile contact.

5. Initial width of grabens, averaging between 80 and 100 m, is a function of the thickness of the brittle plate below the depth of open master joints and the mechanical properties of the rocks.

6. Paired faults initiate simultaneously, and equal displacements occur contemporaneously on each fault.

7. Grabens propagate along strike maintaining a constant initial width between 80 and 100 m.

8. Displacement of the downthrown block is a function of the age of the graben.

9. The initial geometry of large, complex grabens may have been similar to the geometry of simple grabens, though severe geometric problems suggest that at least some of these more complex grabens, in particular Red Lake Canyon graben, may not have been similar to simple grabens when smaller.

10. Grabens are progressively younger eastward from Red Lake Canyon. The relative age of grabens between Red Lake Canyon and Cataract Canyon is not well established.

An outgrowth of this study is a generalized expression for estimating the depth to the flowing layer from surface geometry alone. Evaluation of this expression requires knowledge of the initial width, the change in width, the vertical displacement of the downthrown block, and the fractional increase in the original volume of the downthrown block due to internal failure (bulk dilatancy). It is common in small grabens that the original fault scarps are preserved and the downthrown blocks are exposed. Width and displacement can be measured accurately and the change in width computed if the end width is taken as the initial width. Bulk dilatancy may be assumed negligible for small grabens because the downthrown block is able to fill all the available space beneath the graben floors without internal failure, except for minor shearing and brecciation along the faults and near its base. Thus,

small grabens can be reliable indicators of depth to the flowing layer if the model for graben growth is correct. Most large grabens, on the other hand, have been modified by processes of secondary widening so that even if the assumption of constant initial width is valid, the change in width is difficult to determine. For this reason, and because the downthrown block is commonly buried by an unknown thickness of recent deposits, the expression should not be applied to large grabens.

REFERENCES CITED

Anderson, E. M., 1951, The dynamics of faulting and dyke formation with applications to Britain: 2nd edition, Edinburgh and London, Oliver and Boyd, 206 p.

Baars, D. L., 1962, Permian System of Colorado Plateau: Am. Assoc. Petroleum Geologists Bull., v. 46, p. 149-218.

_____, 1971, Geology of the Canyonlands: in Baars, D. L., and Molenaar, C. M., (eds.), 1971, Geology of Canyonlands and Cataract Canyon, Four Corners Geological Society, 6th Field Conference, Cataract Canyon River Expedition, p. 18-27.

Baker, A. A., 1933, Geology and oil possibilities of the Moab district, Grand and San Juan Counties, Utah: U.S. Geol. Survey Bull. 841, 95 p.

_____, 1946, Geology of the Green River Desert-Cataract Canyon region, Emery, Wayne, and Garfield Counties, Utah: U.S. Geol. Survey Bull. 951, 122 p.

Belousov, V. V., 1961, Experimental geology: Sci. American, v. 204, p. 97-106.

Cloos, E., 1955, Experimental analysis of fractures: Am. Assoc. Petroleum Geologists Bull., v. 66, p. 241-256.

_____, 1968, Experimental analysis of Gulf Coast fracture patterns: Am. Assoc. Petroleum Geologists Bull., v. 52, p. 420-444.

Elston, D. P., and Shoemaker, E. M., 1961, Preliminary structure contour map on top of salt in the Paradox Member of the Hermosa Formation in the salt anticline region, Colorado and Utah: U.S. Geol. Survey Oil and Gas Investigations, Map OM 209.

_____. 1963, Salt anticlines of the Paradox Basin, Colorado and Utah: in Symposium on salt: Northern Ohio Geol. Soc., p. 131-146.

Gregory, H. E., 1938, The San Juan Country, a geographic and geologic reconnaissance of parts of Arizona, New Mexico, and Utah: U.S. Geol. Survey Prof. Paper 188, 123 p.

Hafner, W., 1951, Stress distributions and faulting: Geol. Soc. America Bull., v. 62, p. 373-398.

Handin, J., 1966, Strength and ductility: in Handbook of Physical Constants, Geol. Soc. American Mem. 97, p. 273-274.

Harrison, T. S., 1927, Colorado-Utah salt domes: Am. Assoc. Petroleum Geologists Bull., v. 11, p. 111-133.

Hollingsworth, S. E., Taylor, J. H., and Kellaway, G. A., 1944, Large-scale superficial structures in the Northampton Ironstone Field: Geol. Soc. London Quart. Jour., v. 100, pt. 1-2, p. 1-44.

Hubbert, M. K., 1937, Theory of scale models as applied to geologic structures: Geol. Soc. America Bull., v. 48, p. 1459-1521.

_____, 1951, Mechanical basis for certain familiar geologic structures: Geol. Soc. America Bull., v. 62, p. 355-372.

Hunt, C. B., 1956, Cenozoic geology of the Colorado Plateau: U.S. Geol. Survey Prof. Paper 279, 99 p.

Kelley, V. C., and Clinton, N. J., 1960, Fracture systems and tectonic elements of the Colorado Plateau: University of New Mexico Publications in Geology, no. 6, 104 p.

Lewis, R. Q., Sr., and Campbell, R. H., 1965, Geology and uranium deposits of Elk Ridge and vicinity, San Juan County, Utah: U.S. Geol. Survey Prof. Paper 474-B, 69 p.

Link, T. A., 1930, Experiments related to salt-dome structures: Am. Assoc. Petroleum Geologists Bull., v. 14, p. 483-503.

Lohman, S. W., 1974, The geologic story of Canyonlands National Park: U.S. Geol. Survey Bull. 1327, 126 p.

McGill, G. E., and Stromquist, A. W., 1974, A model for graben formation by subsurface flow: Canyonlands National Park, Utah: Department of Geology and Geography, University of Massachusetts, Contribution no. 15, 79 p.

Mutschler, F. E., and Hite, R. J., 1969, Origin of the Meander anticline, Cataract Canyon, Utah; and basement fault control of Colorado River drainage(abs.): Geol. Soc. America Abstracts with Program for 1969, pt. 5, p. 57-58.

Nettleton, L. L., and Elkins, T. A., 1947, Geologic models made from granular materials: Am. Geophys. Union Trans., v. 28, p. 451-466.

Nye, J. F., 1952, Mechanics of glacier flow: Jour. Glaciology, v. 2, p. 82-93.

_____, 1965, The flow of a glacier in a channel of rectangular, elliptical, or parabolic cross section: Jour. Glaciology, v. 5, p. 661-690.

Parker, T. J., and McDowell, A. N., 1951, Scale models as a guide to interpretation of salt-dome faulting: Am. Assoc. Pétroleum Geologists Bull., v. 35, p. 2076-2086.

_____, 1955, Model studies of salt-dome tectonics: Am. Assoc. Petroleum Geologists Bull., v. 39, p. 2384-2470.

Powell, J. W., 1875, Exploration of the Colorado River of the West and its tributaries: Washington, D.C., U.S. Govt. Printing Office, 291 p.

Price, N. J., 1974, The development of stress systems and fracture patterns in undeformed sediments: Denver, Procedings of the Third Congress of the International Society for Rock Mechanics, v. 1, pt. A, p. 487-496.

Prommel, H. W. C., and Crum, H. E., 1927, Salt domes of Permian and Pennsylvanian age in southeastern Utah and their influence on oil accumulation: Am. Assoc. Petroleum Geologists Bull., v. 11, p. 373-393.

Sanford, A. R., 1959, Analytical and experimental study of simple geologic structures: Geol. Soc. America Bull., v. 70, p. 19-52.

Tanner, W. F., and Williams, G. K., 1968, Model diapirs, plasticity, and tension: in Braunstein, J., and O'Brien, G. D.(Eds.), Diapirs and diapirism: Am. Assoc. Petroleum Geologists, Mem. 8, p. 10-15.

Timoshenko, S., and Goodier, J. N., 1951, Theory of elasticity: New York, McGraw Hill, p. 11-13.

PLATE I GEOLOGIC MAP OF THE LOWER RED LAKE CANYON AREA, CANYONLANDS NATIONAL PARK, UTAH

EXPLANATION

DESCRIPTION

RECENT

Qa — Unconsolidated talus, alluvium, colluvium, and eolian material.

PERMIAN

Pcm — CEDAR MESA SANDSTONE MEMBER OF THE CUTLER FORMATION
Thick-bedded calcareous sandstone interlayered locally with lensoidal gray limestone.

Pr — RICO FORMATION
Alternating beds of red to buff calcareous cross-bedded sandstone, red shale, purple and gray siltstone, and thin gray limestone.

PENNSYLVANIAN

IPuh — UPPER MEMBER OF THE HERMOSA FORMATION
Thin-bedded to massive gray limestone containing abundant invertebrate fossils and chert nodules, interbedded with crossbedded gray calcareous sandstone and thin-bedded gray calcareous shale.

IPp — PARADOX MEMBER OF THE HERMOSA FORMATION
Bedded gypsum and limestone with minor amounts of siltstone and shale.

SYMBOLS

U
D

NORMAL FAULT
Solid where fault is accurately located, dashed where approximately located, dotted where location is inferred. U, upthrown side. D, downthrown side.

THRUST FAULT
Hachures drawn on the upthrown side.

CONTACT
Solid where contact is accurately located, dashed where approximately located, dotted where location is inferred.

6
STRIKE AND DIP OF BEDDING

METERS 0 200 400 600 800 1000
FEET 0 1000 2000 3000

TOPOGRAPHIC CONTOUR INTERVAL = 40 FT.
DATUM IS MEAN SEA LEVEL

Topographic map is a portion of the U.S.G.S. (1955) Carlisle 3 NE & NW 7½" topographic quadrangles published at a 1:24000 scale.

N MN 15°

109° 55' 109° 52' 30" 38° 10'

COLORADO CANYON RIVER
Spanish Bottom
Lower Red Lake Canyon
Twin Canyon
Red Lake Canyon
Cyclone Canyon
CATARACT
Lens

PLATE 2 GEOLOGIC STRUCTURE SECTIONS

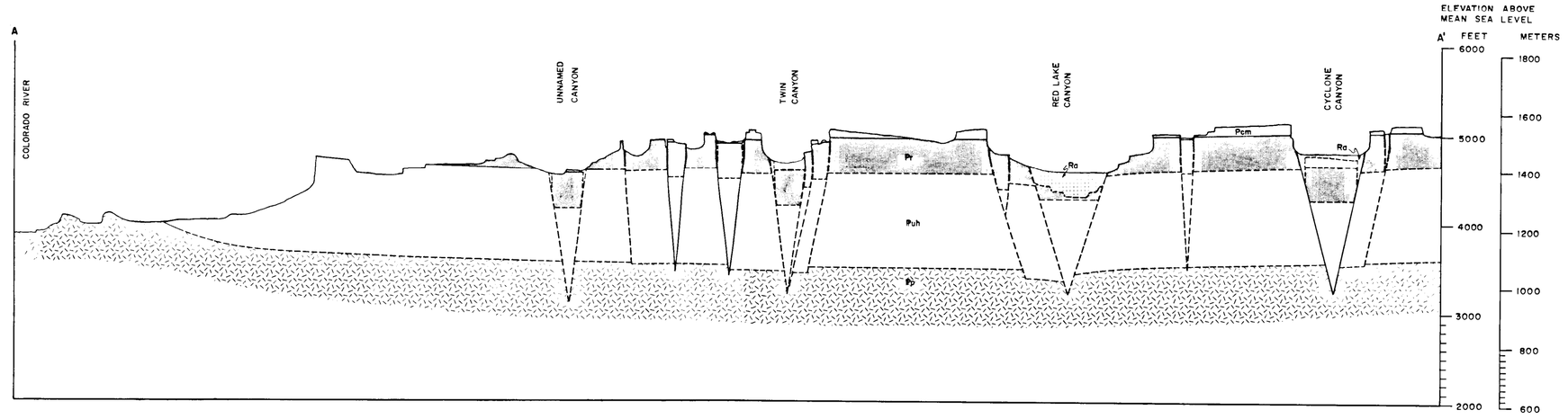

SCALE: HORIZONTAL= VERTICAL

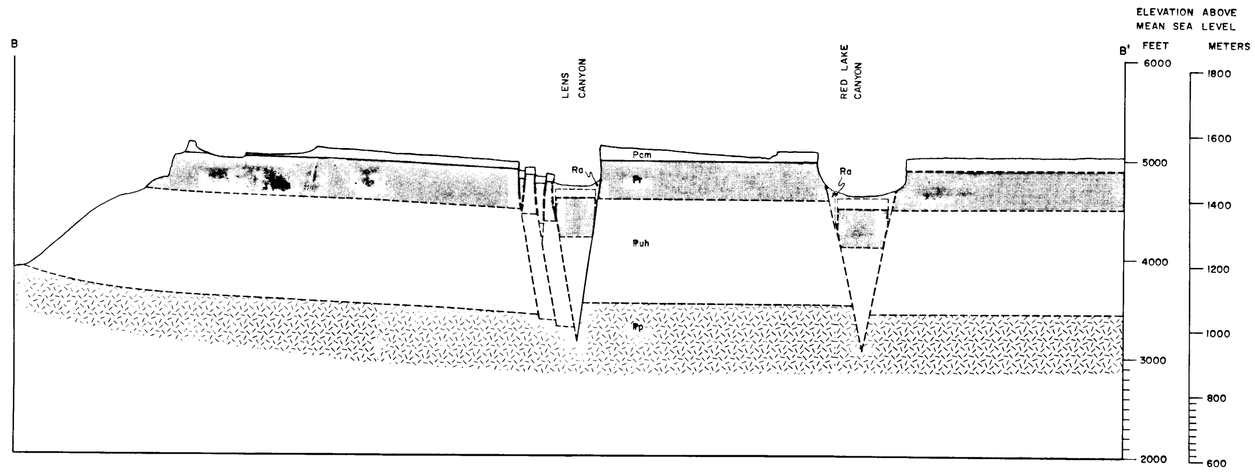

EXPLANATION

- Ra — Undifferentiated alluvium, colluvium, talus and eolian material
- Pcm — Cedar Mesa Sandstone Member of the Cutler Formation
- Pr — Rico Formation
- Puh — Upper member of the Hermosa Formation
- Pp — Paradox Member of the Hermosa Formation